COHERENT PRODUCTION ON NUCLEI BY π AND K MESONS (EXPERIMENT)

By W. Beusch

CERN, Geneva*

(Presented at the XII Cracow School of Theoretical Physics, Zakopane, June 8–18, 1972)

In these lectures some experimental methods useful for detecting coherent processes are compared. Experimental results of coherent production by π and K mesons are discussed. High statistics results were obtained from a counter experiment performed at CERN. The optical model for multiple scattering is shown to fit the data of 3π, 5π, and $K\pi\pi$ production very well, while some doubts as to its application to $K^*(890)$ production remain. The main results of the analysis are the following. The absorption of 3π and 5π systems in nuclear matter is small; it corresponds to a total cross-section $\sigma \approx 25$ mb. Mass distributions of 3π, 5π and $K\pi\pi$ show broad structureless peaks. Both 3π and $K\pi\pi$ are almost 100% two-body systems with $\pi\varrho$ and πf for 3π and $K^*(890)\pi$ in $K\pi\pi$ (no $K\varrho$ observed). The 3π Dalitz plot distributions show structure within the $J^P = 1^+$ amplitude, possibly $S-D$ interference of the $\pi-\varrho$ state. The production cross-section of 3π on a nucleon, deduced from a fit over nine target elements, seems to rise by 30% from 9 to 15 GeV, while the absorption in nuclear matter appears unchanged.

Coherent production of $K^*(890)$, a non-diffractive process, is clearly observed. A model for this process including Coulomb production, strong production, and their interference, is discussed. A fit to 10 data points, the integrated coherent production cross-sections on five elements and three beam momenta, gives $0 < \Gamma(K^* \to K\gamma) < 80$ keV.

1. Introduction

These lectures will cover the following experiments

$$\pi^- + A \to \pi^+\pi^-\pi^- + A \quad \text{and} \quad \pi^- + A \to 2\pi^+ 3\pi^- + A$$

$$K^+ + A \to K^+\pi^+\pi^- + A \quad \text{and} \quad K^+ + A \to K^*(890) + A.$$

The experimental data are mainly those of a high statistics counter experiment done at CERN [1–3]. In this experiment three beam momenta (9, 12, 15 GeV/c) and nuclei with $9 \leqslant A \leqslant 207$ were used. For the analysis of these data an optical model, *i.e.* the large A approximation of the Glauber multiple scattering theory, is used [4]. While the model for 3π production will not be derived, the properties of the model for coherent $K^*(890)$ production

* Address: CERN, 1211 Genève 23, Switzerland.

on nuclei will be discussed in some detail. Numerical computations of this model show that a simplification, used previously, is not valid.

The largest part of these lectures will be devoted, however, to the discussion of experimental results. Experimental methods used to verify the coherence of interactions on nuclei will be briefly reviewed at the beginning. Throughout the lectures I shall point out experimental difficulties — also errors in the analysis that have been detected — in an attempt to give some feeling of the work of experimentalists to the audience of this School on theoretical physics. I hope that nobody in this audience has ever tried to explain an experiment that later turned out to be wrong; such things do happen, however, and they must be very frustrating indeed. More dialogue between experimentalists and theoreticians could probably prevent such accidents, and I feel this school is a good place for such a dialogue.

The advantages of nuclear targets for studying diffractive processes are well known to this audience. The average high-energy physicist does not like them. He thinks experiments on nuclei are "dirty": one loses constraints in the kinematics due to Fermi momentum and excitation energy, and there may be multiple interactions. In selecting coherent interactions these disadvantages disappear and there remain advantages for studying diffractive systems:

(*i*) no spin flip, no N^* production of the target,

(*ii*) states with $J^P = 0^-, 1^+, 2^- \ldots$ (and helicity 0) only for incident π and K,

(*iii*) simplified analysis (follows from (*i*) and (*ii*)),

(*iv*) measurement of the propagation of diffractive systems through nuclear matter, and

(*v*) high electric field for Coulomb production.

Properties (*i*) and (*ii*) are strictly valid only if the target nucleus remains "untouched" (no excitation, no spin flip, no isospin charge). This is rather difficult to verify experimentally. In coherent production, processes in disagreement with properties (*i*) or (*ii*) vanish for heavy nuclei (of order $1/A$); they are negligible in the experiments discussed here.

2. Detection of coherence

2.1. Detection of coherence event by event

A measurement on the recoiling nucleus is needed. The kinetic energy of the target nucleus T_A of mass M_A is given by

$$-t = 2M_A \cdot T_A.$$

If the recoiling nucleus has to be measured in some way one is restricted to the lightest nuclei, d and ^{4}He [5]. Nature works against the use of this method with heavy nuclei in three ways: smaller t values are needed for heavier nuclei, heavy nuclei get less kinetic energy, and the range of heavier nuclei gets smaller. A ^{4}He nucleus recoils at a value of t as large as $-t = 0.04\,(\mathrm{GeV}/c)^2$, with a kinetic energy of slightly more than 5 MeV, and has a range of about 20 cm in He gas at atmospheric pressure. It is evident, from this example, that the observation of the recoil of heavier nuclei is rather hopeless. A possible

exception to this rule may be Si or Ge whose recoil energy can, in principle, be measured in a solid-state counter made of these elements. Instead of detecting the recoil nucleus and measuring its mass from momentum and range, or from energy and specific energy loss, one may compute the missing mass of the nucleus from a precise measurement of all other momenta. Excitation or break-up of the nucleus would manifest itself in an increase of this missing mass. The error Δmm of this quantity is given by

$$\Delta\text{mm} \simeq \Delta(E_i - E_f),$$

E_i being the energy of the incident particle and E_f the energy of the outgoing system. Errors Δmm $\sim$ 1 MeV are needed, a precision not available in the 10–20 GeV region. This method has worked beautifully, however, for elastic scattering of protons on nuclei

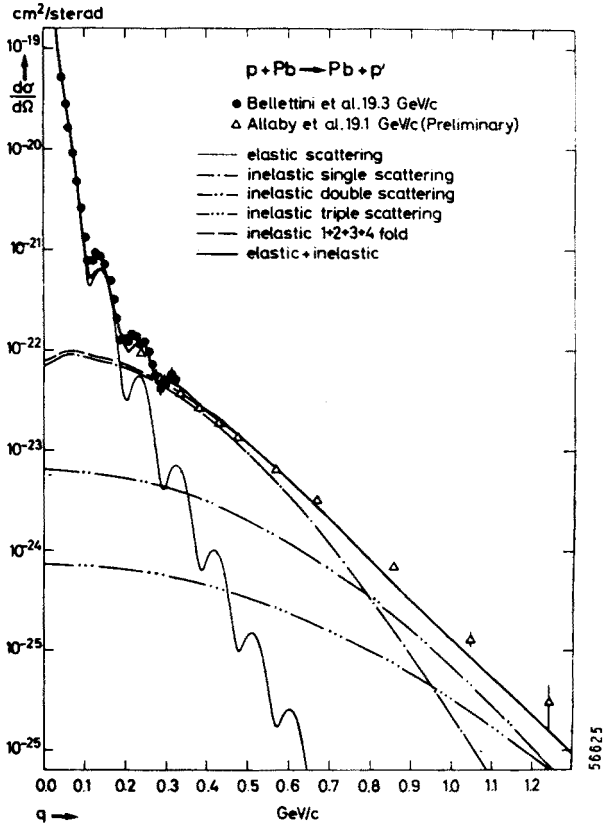

Fig. 1. Angular distribution of protons scattered from Pb [7]. The curves are the result of a multiple scattering calculation by Kofoed-Hansen

at 1 GeV [6]. At 19 GeV/c an experiment on proton-nucleus elastic scattering [7] was no longer able to separate quasi-elastic from coherent events. (But the theory can account for this deficiency very well, see Fig. 1.) An experiment on proton-elastic scattering can take advantage of the ejected beam of a proton synchrotron which is of high

quality (large $d^2N/dpd\Omega$). Moreover, due to the kinematics of elastic scattering and the high beam flux, only a small solid angle for the measurement of the elastically scattered protons is needed. A coherent production experiment with incident π or K mesons is at a disadvantage in both respects: momentum and direction of the incident beam have a larger spread, and the multi-particle final state demands a large acceptance. For a given accuracy the cost of a spectrometer goes up at least proportional to the accepted solid angle. A measurement precision sufficient to detect nuclear excitation is therefore virtually impossible.

2.2. Statistical separation of coherent and incoherent events

This method works best for small t values and heavy nuclei where the signal-to-noise ratio is about 30:1. The success of this method will be clear from the discussion of the experiments.

2.3. Event rates

Helium at atmospheric pressure is not a dense target material, in fact most experimentalists use He bags as a reasonable substitute for vacuum. 4×10^{10} particles produce one event for a cross-section of 1 μb and a target length of 1 cm. I estimate the cross-section for A_1 production at the first diffraction minimum to be $d\sigma/dt = 5$ μb/(GeV/c)^2. Choosing bin widths $\Delta t = 0.02$ (GeV/c)^2 and $\Delta M(3\pi) = 100$ MeV ($\approx \frac{1}{2}$ of the A_1 width), the cross-section of this particular bin is ≈ 0.05 μb. 8×10^{11} incident π mesons are needed if 100 events are wanted in this bin and if the effective target length is 1 m. The He recoil energy in this region is $T = 50$ MeV and He pressure higher than atmospheric can be used.

Liquid deuterium is a much denser target material than He gas. In elastic scattering d recoils have been observed from $-t = 0.2$ (GeV/c)^2 with a conventional spark chamber set-up [8]. This experiment explores the single-double scattering interference region. Exploring this region in coherent A_1 production would allow a rather direct measurement of A_1-nucleon scattering. The cross-section is of the order $d\sigma/dt = 0.1$ μb/(GeV/c)^2. Using bins of $\Delta M(3\pi) = 100$ MeV and $\Delta t = 0.1$ (GeV/c)^2 leads to an estimated bin cross-section of 5×10^{-3} μb. In order to observe again 100 events in this bin 10^{10} pions have to go through a 50 cm long D_2 target. In reality only 10% of the solid angle may be covered with recoil detectors and 10^{11} incident particles are needed in this case. While counter experiments with 10^{11} incident particles are not impossible — they would take about one year — there is another aspect not to be forgotten: data analysis. In the last deuterium example, the total number of interactions will be 10^{10}. Since a precise momentum analysis of four charged particles is involved, an event takes roughly 1 sec on a fast computer. A trigger system has to suppress unwanted events in the ratio $1:10^4$, in order to reduce the analysis load to a manageable amount. It is quite an art to set up such a trigger system that does not severely bias the wanted events as well. The technical possibilities exist, however, and if the theoreticians can convince counter physicists of the interest of the subject such experiments may be undertaken some day.

Bubble chamber experiments are not sensitive to such small cross-sections; a large

exposure is limited to about 10^7 incident particles, four orders of magnitude below a counter experiment. This ratio shrinks to two orders of magnitude if minority particles of a beam ($K^{\pm}, \bar{p}$) are considered.

3. Coherent production of 3π and 5π systems on nuclei

3.1. Experimental considerations

The CERN-ETH-Imperial College Group had used a magnet spark chamber system for many years [9]. The shape of the magnet ($60 \times 66 \times 160$ cm^3 useful volume), with the longest dimension along the beam, was quite well adapted to a coherent production experiment: the target region need not be observed; it can therefore be outside the magnet.

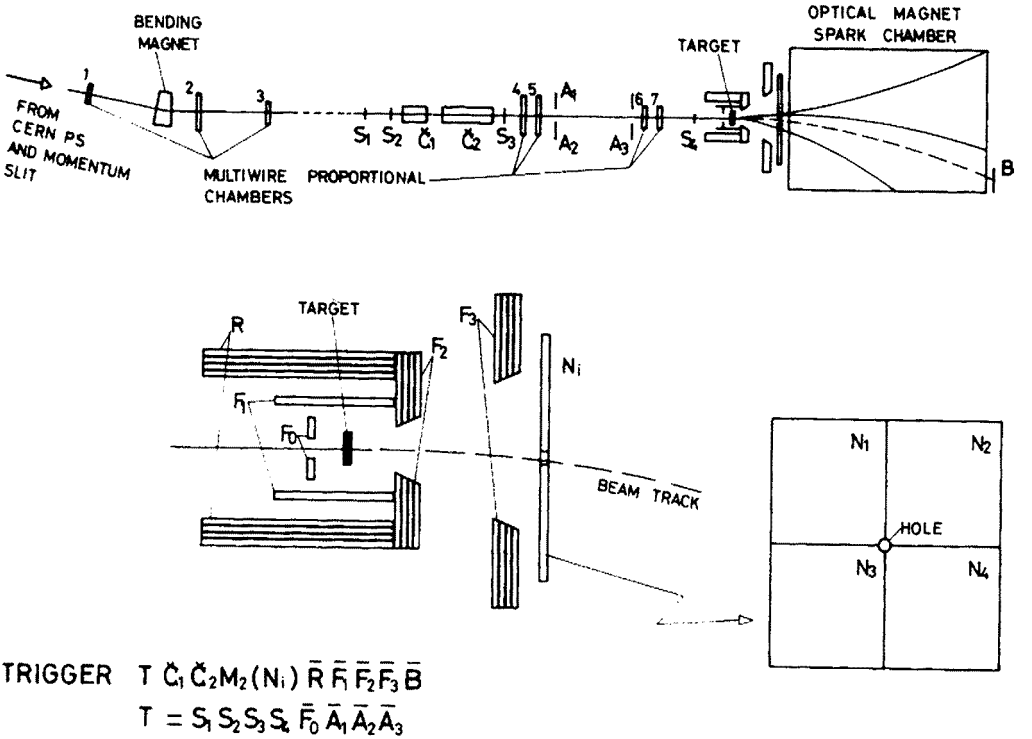

Fig. 2. Schematic diagram of the experimental set-up at the CERN Proton Synchrotron. In the lower part the anticoincidence counters (R, F) and multiplicity counters (N_i) are shown enlarged

The average track length in the spark chambers is almost the full 160 cm, since the final state particles are so much collimated into the forward direction. The experimental set-up is shown in Fig. 2 [1]. The target region was not quite unobserved; it was surrounded, in fact, almost completely by veto counters detecting charged particles and γ-rays from π^0 (F_1, R, F_2 and F_3 in Fig. 2). Only a cone of $\pm 20°$ was left open in the forward direction, where the three of five charged pions were observed. With the counters enumerated so

far, this trigger system would accept not only all coherent events, but also elastic scattering and events with no interaction. Coherent production is selected by further demanding at least two particles inside the forward cone of $\pm 20°$; this is done by counting the number of hits in counters N_1 to N_4. With this trigger condition one still observes mostly beam tracks. The beam particle hits one counter N_i. If it also produces a δ-ray of $\geqslant 1$ MeV this will curve in the magnetic field and hit another counter N_j. This effect is one of the many surprises the experimental physicists have when setting up a large acceptance trigger system. It was avoided by having a hole in the N_i counter, and a veto counter B in the beam line behind the magnet, and by carefully adjusting counters $S_1, \ldots, S_4, F_0$, the hole in N_i, and B, to the envelope of the beam. We finally reached a trigger probability of 2×10^{-5} for non-interacting particles.

I have explained this trigger system in some detail as an illustration of the fact that in counter experiments a balance between the rate of useless triggers (that load the data processing system) and experimental biases must be found. In our case the bias is rela-

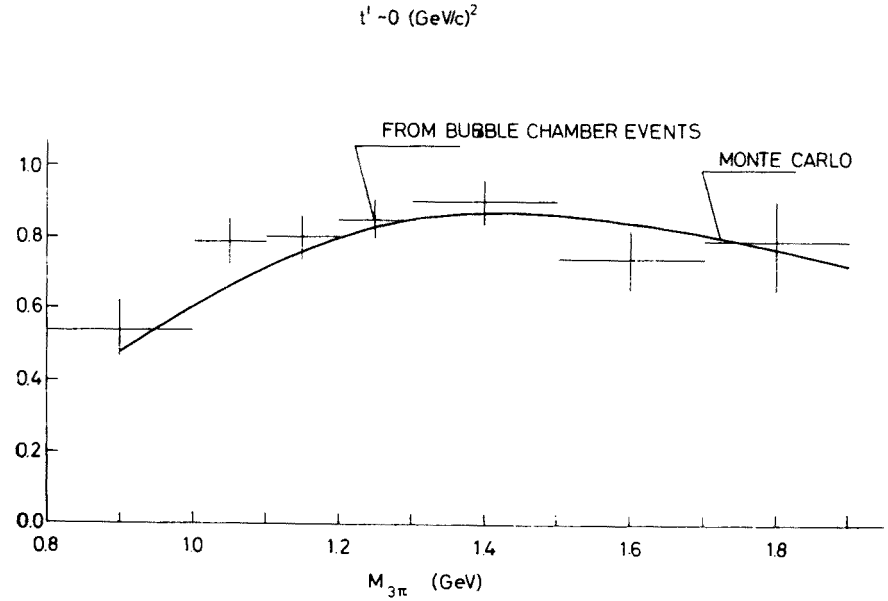

Fig. 3. Detection efficiency of 3π coherent production events as a function of the 3π mass

tively mild (see Fig. 3 for acceptance *versus* 3π mass). Mainly responsible for the losses are the hole in the N_i counters at low 3π mass and the $\pm 20°$ angle limitation at high 3π mass.

The separation of coherent production from incoherent reactions turns out to be quite acceptable. The sharp forward peak rises a factor 30 to 100 over the incoherent background. This is a consequence of the relatively small absorption of mesons in nuclear matter. The observation of the forward peak and diffraction pattern is only possible, however, if the resolution on the scattering angle is adequate. Figure 4 shows the deformation of the theoretical diffraction pattern (given as $d\sigma/dq_\perp$, where $\Delta q_\perp \sim p_{\text{lab}} \Delta\theta_{\text{lab}}$) by

the experimental resolution. It shows that the diffraction pattern on Pb has almost disappeared when the error on the scattering angle is $\Delta\theta_{lab} = \pm 2$ mrad. We estimate our error to be $\Delta\theta_{lab} \simeq \pm 1.2$ mrad.

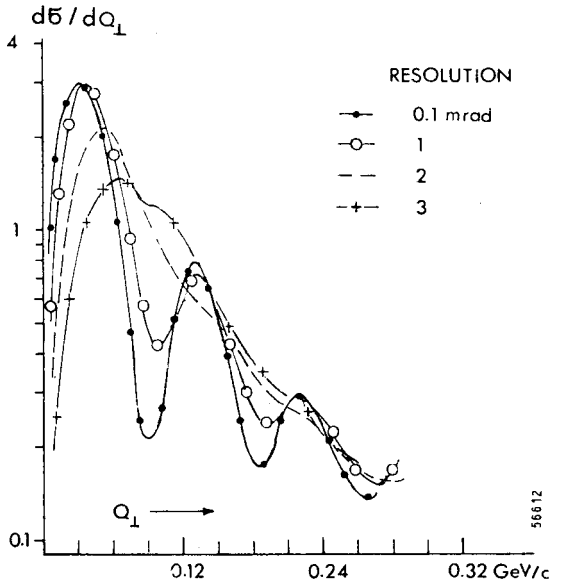

Fig. 4. Calculated distortion of the diffraction pattern for $\pi^- \text{Pb} \to 3\pi \text{Pb}$, at 15 GeV/$c$, as a function of the resolution in the laboratory scattering angle

3.2. Experimental data and their interpretation

The experimental data on many nuclei show a very impressive regular pattern in the t' distribution[1] shown in Fig. 5. We are here in an unusual situation in strong interaction physics since we have a very reliable theory to extract interesting parameters from these data. The theory is so reliable, because the nucleus acts as a large, passive target whose matter distribution determines the angular distribution and — *via* absorption — the A dependence of coherent production.

I assume the reader to be familiar with the Glauber multiple scattering theory and its heavy nuclei limit, the optical model. The observed angular distribution, $d\sigma/dt'$ (exp), is

$$d\sigma/dt'\,(\text{exp}) = d\sigma/dt'\,(\text{coh}) + d\sigma/dt'\,(\text{incoh}). \tag{1}$$

$d\sigma/dt'$ (incoh) is essentially the distribution observed on free nucleons. It has been suggested [10] that the incoherent production in the forward direction is suppressed by the Pauli exclusion principle (no nuclear final states available for small momentum transfers). Fits to our data do not require such a suppression factor and it has been neglected; its inclusion would not significantly change any result. The veto counters of the trigger system produce a bias on the incoherent events; recoil protons of sufficient energy are

[1] As usual $t' = t - t_{min}$. In the following text, t' is sometimes taken as a positive number.

detected and these events are therefore suppressed. This bias was not included in Ref. [1]; its inclusion improves the fit significantly and changes the results within the systematic errors given in Ref. [1]. Its effect can be seen in Fig. 5 as a transition from background curve *II* to curve *I* at a t' value dependent on the proton absorption in the target. The targets thicknesses were chosen such that multiple scattering errors were constant, *e. g.*

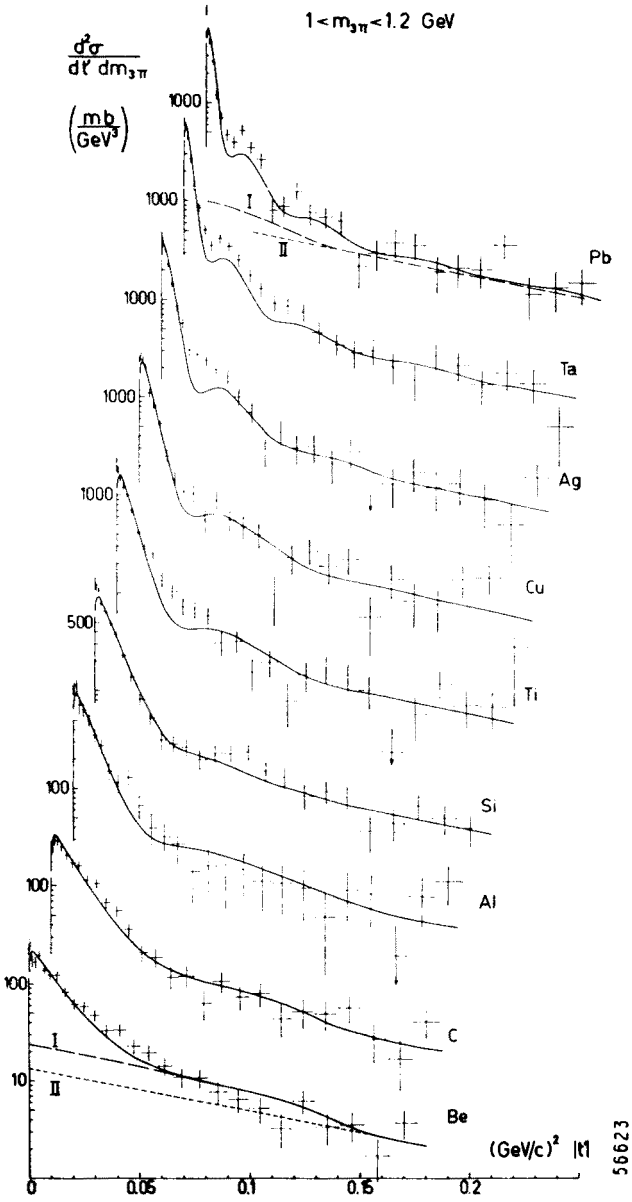

Fig. 5. Differential cross-section $d^2\sigma/dt'dm_{3\pi}$ for different target nuclei and for produced masses in the interval 1.0–1.2 GeV

2.55 cm for Be, 0.05 cm for Pb. We did not attempt to use any model for incoherent production relating the different target nuclei, but treated the incoherent subtraction individually for all A.

We have computed the coherent differential cross-section from [4]

$$\frac{d\sigma}{dt}(\text{coh}) = C(t', M)A^2|\tilde{F}(t', A, M\ldots)|^2, \tag{2}$$

where $C(t', M) = C_0(M)\exp\{Bt'\}$ is the diffractive production amplitude for a system of mass M, B is the slope of the corresponding t' distribution. Coherent production on nuclei is a clean way of projecting out diffractive production. $C_0(M)$, a result of the fit over all elements, can therefore be compared to other methods of extracting the diffractive part of the production on free protons.

The optical model approximation for the form factor $\tilde{F}$ can be understood in a simple geometrical and probabilistic way (see Fig. 6). All vectors are decomposed into a longitudinal part $Q_{||}$, z and a transverse part $\vec{Q}_\perp$, $\vec{b}$. If the production takes place at the point

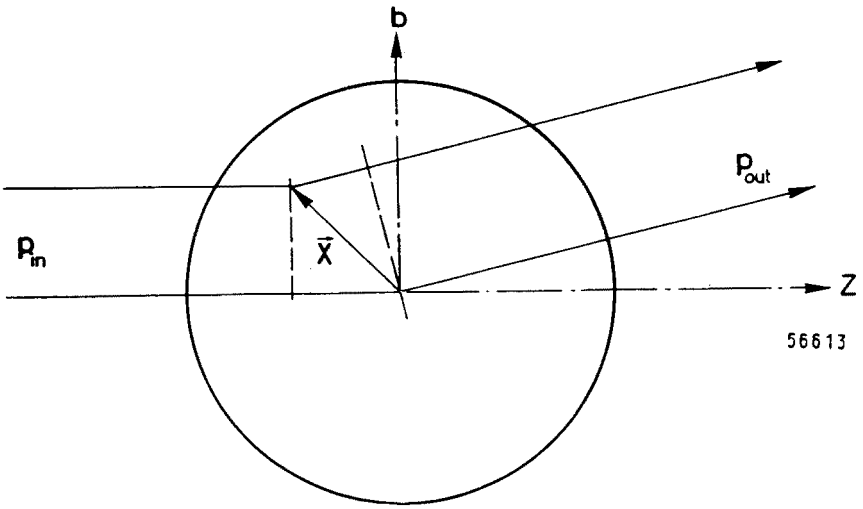

Fig. 6. Geometrical optics inside the nucleus

$\vec{x} = \{\vec{b}, z\}$ the outgoing wave has a phase difference $\Delta\varphi$ with respect to production at the centre of the nucleus ($\vec{x} = 0$)

$$\Delta\varphi = \vec{p}_{in}\cdot\vec{x} - \vec{p}_{out}\cdot\vec{x} = \vec{Q}\cdot\vec{x} = \vec{Q}_\perp\cdot\vec{b} + Q_{||}z.$$

The incident wave has a probability amplitude for survival up to z which is

$$\exp\{-\tfrac{1}{2}\sigma_1(1-i\alpha_1)\int_{-\infty}^{z} A\varrho(b, z)dz\} = \exp\{-\tfrac{1}{2}\sigma_1(1-i\alpha_1)T_1(b, z)\}.$$

This probability amplitude is composed from a damping factor, $\exp\{-\frac{1}{2}\sigma_1 T_1(b, z)\}$, and it also contains a phase rotation, $\Delta\varphi_1(b, z)$, which is proportional to α_1, the ratio of

the real to the imaginary part of the forward scattering amplitude: $\Delta\varphi_1(b, z) = \frac{1}{2}\sigma_1\alpha_1 \times$ $\times T(b, z)$.

Treating the outgoing wave the same way (parameters $\sigma_2, \alpha_2, T_2 = \int_z^\infty A\varrho(b, z)dz$) and setting the production amplitude proportional to the nuclear matter in the volume element ($\sim \varrho(b, z)\, d^2\vec{b}\, dz$) one can immediately write down

$$\tilde{F}(t', A\ldots) = \int e^{i(\vec{Q}_\perp\vec{b}+Q_\parallel z)} \times e^{-\frac{1}{2}\sigma_1(1-i\alpha_1)T_1(b,z)} \times$$
$$\times e^{-\frac{1}{2}\sigma_2(1-i\alpha_2)T_2(b,z)}\varrho(b, z)d^2\vec{b}dz. \tag{3}$$

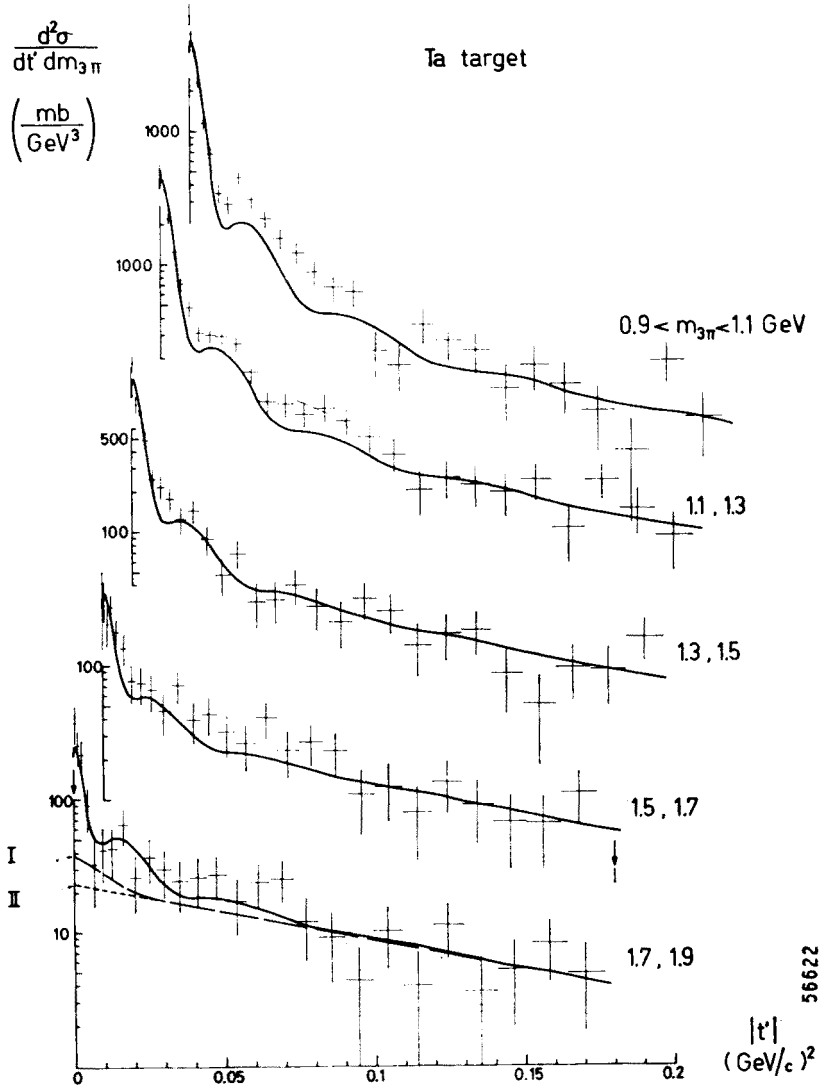

Fig. 7. Differential cross-section $d^2\sigma/dt'dm_{3\pi}$ for different mass intervals and for the target nucleus Ta

For the nucleon number density $\varrho(b, z)$, we used the Woods-Saxon model

$$\varrho(r) = \frac{\varrho_0}{1+\exp\left(\frac{r-c}{a}\right)}, \quad \int \varrho(r) d^3\vec{r} = 1 \tag{4}$$

and the parameters $c = 1.12 \text{ fm} \cdot A^{\frac{1}{3}}$, $a = 0.545$ fm.

Inserting Eqs (2) and (3) into Eq. (1) and folding in also the resolution correction, one obtains a model that can be compared to the experimental data $d\sigma/dt$ (exp). This comparison is shown in Figs 5 and 7. All parameters, except a scale parameter in $d\sigma/dt'$ (incoh) and the scale parameter $C_0(M)$ in $d\sigma/dt$ (coh), have been kept fixed: ($\sigma_1 = 25.4$ mb, $\alpha_1 = -0.1$, $\sigma_2 = 25$ mb, $\alpha_2 = 0$). The model is in excellent agreement with the data over a large range of t', A, and $M(3\pi)$. The scale parameter $C_0(M)$ turns out to be almost independent of A, indicating that $\sigma_2 = 25$ mb is a reasonable choice for the absorption of three pions in nuclear matter. A similar fit leaving σ_2 to be fitted, but $C_0(M)$ constrained to be the same for all A, would have required excessive computer time. We therefore determined σ_2 from integrated coherent cross-sections, σ_{coh}, where

$$\sigma_{\text{coh}}(A, M_1, M_2) = \int_{M_1}^{M_2} dM \int_0^{t'^*} dt' \frac{d^2\sigma(\text{coh})}{dM dt'}, \tag{5}$$

and where the cut-off value t'^* was approximately at the first maximum of the distribution. It was obviously chosen the same for the experimental and for the theoretical cross-section. In Ref. [1], the incoherent subtraction did not contain the proton recoil bias; the more recent fits of σ_2 presented here are therefore slightly different from those given in Ref. [1] (they are roughly at the lower limit allowed by the systematic error). The comparison of the model with the data with respect to the A dependence of σ_{coh} for different mass bins is shown in Fig. 8 and the best fit values of σ_2 are collected in Table I.

The same analysis, in a preliminary form, has been performed for data taken at 8.9 and 13 GeV/c; at 13 GeV/c we have only data on C and Ag. The model fits these data equally well; no difference turns up, except that expected from the larger parallel momentum transfer $Q_{||}$. The best fit values of σ_2 at 8.9 GeV/c are also shown in Table I. No significant energy dependence of σ_2 can be observed.

At 15.1 GeV/c we also have a reasonable sample of coherently produced 5π events. Figure 9 shows a sample of the t' distributions that also exhibits a clear coherence signal in the form of a sharp forward peak. The model was also fitted in this case with a view to obtaining σ_2 for the 5π system. Surprisingly enough, this value also turns out to be near the π-nucleon cross-section (see Table II).

At this point, I would like very much to give you the reason why 3π and 5π systems are so little absorbed in nuclear matter. One can obviously speculate that these systems are still the quark-antiquark pair of the incident pion when they propagate through the nucleus, pure a cross-section similar to the $\pi - N$ cross-section in then expected. This speculation involves (*i*) the quark model, (*ii*) diffractive excitation of broad $q\bar{q}$ states, and (*iii*) suf-

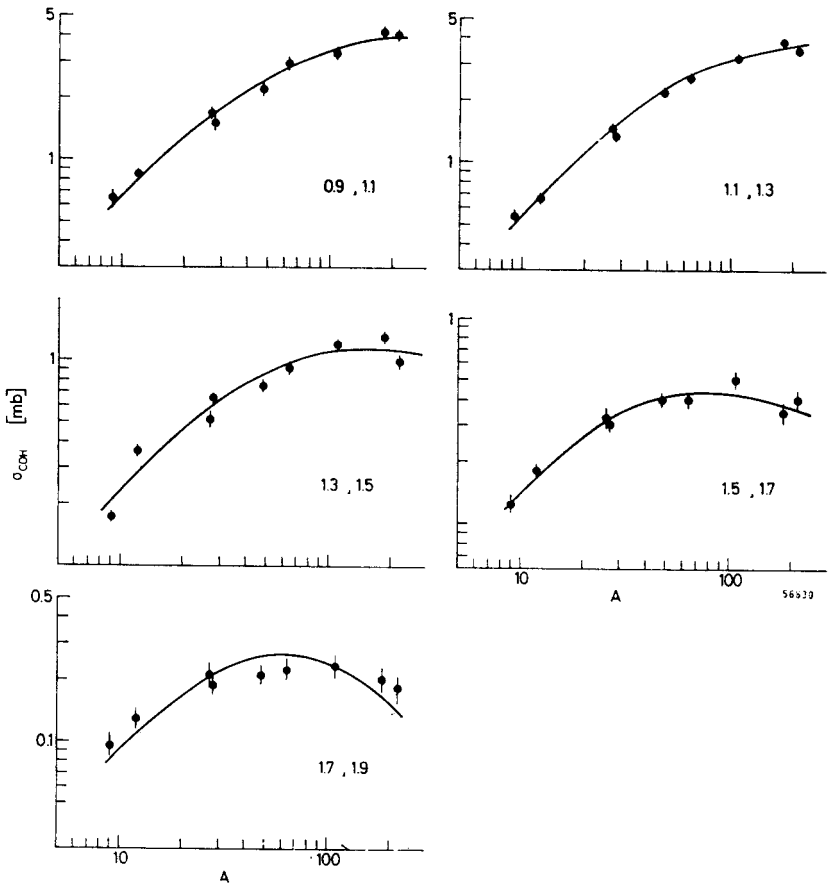

Fig. 8. Best fit optical model curves for σ_{coh} for 3π production for five mass bins as indicated. For best fit parameters, see Table I

TABLE I

Best fit values of the total cross-section σ_2 of the coherently produced 3π system on a nucleon. Errors given are statistical errors only

Mass bin (GeV)	σ_2 (mb)	
	9 GeV/c	15 GeV/c
0.9, 1.1	29 ± 2	28 ± 2
1.1, 1.3	22 ± 2	21 ± 2
1.3, 1.5	5^{+3}_{-2}	21 ± 3
1.5, 1.7	—	23 ± 4
1.7, 1.9	—	13 ± 8

ficiently long lifetime of these states. At 9 GeV/c, the time taken by a system of 1.2 GeV mass to cross one half the thickness of a Pb nucleus (6.5 fm) is $\tau = 2.9 \times 10^{-24}$ sec or $1/\tau = 230$ MeV (relativistic time dilatation included). The observed mass distribution is rather wider than 230 MeV and in this case one would expect σ_2 to be larger at 9 than at

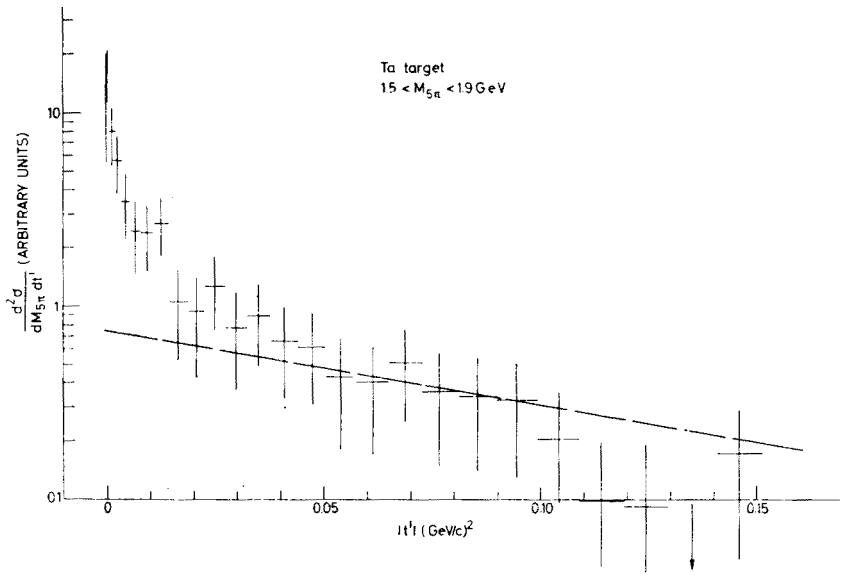

Fig. 9. Angular distribution $d\sigma/dt'$ for Ta target and for produced 5π masses in the interval 1.5–1.9 GeV

TABLE II

Best fit values of the total cross-section σ_2 of the coherently produced 5π system on a nucleon, from Ref.[1]

Mass bin (GeV)	σ_2 (mb)	Statist. error (mb)	System. error (mb)
1.5, 1.7	10	±7	$^{+8}_{-4}$
1.7, 1.9	13	±10	$^{+9}_{-6}$

15.1 GeV/c where less decays of the excited $q\bar{q}$ system take place inside the nucleus. It seems that we face the difficult task of understanding the total cross-section of a system of strongly interacting hadrons on nucleons. The models of diffractive production, discussed by Professors Czyż, Dalitz and Byers at this School, may eventually solve this problem; another approach will be discussed by Professor Gottfried at this School. It is also possible that more experiments are needed (*e. g.* coherent production on deuterium, where single and double scattering can be experimentally observed) to understand this effect. This problem is certainly remarkable in the sense that it is very easy to formulate and very difficult to solve.

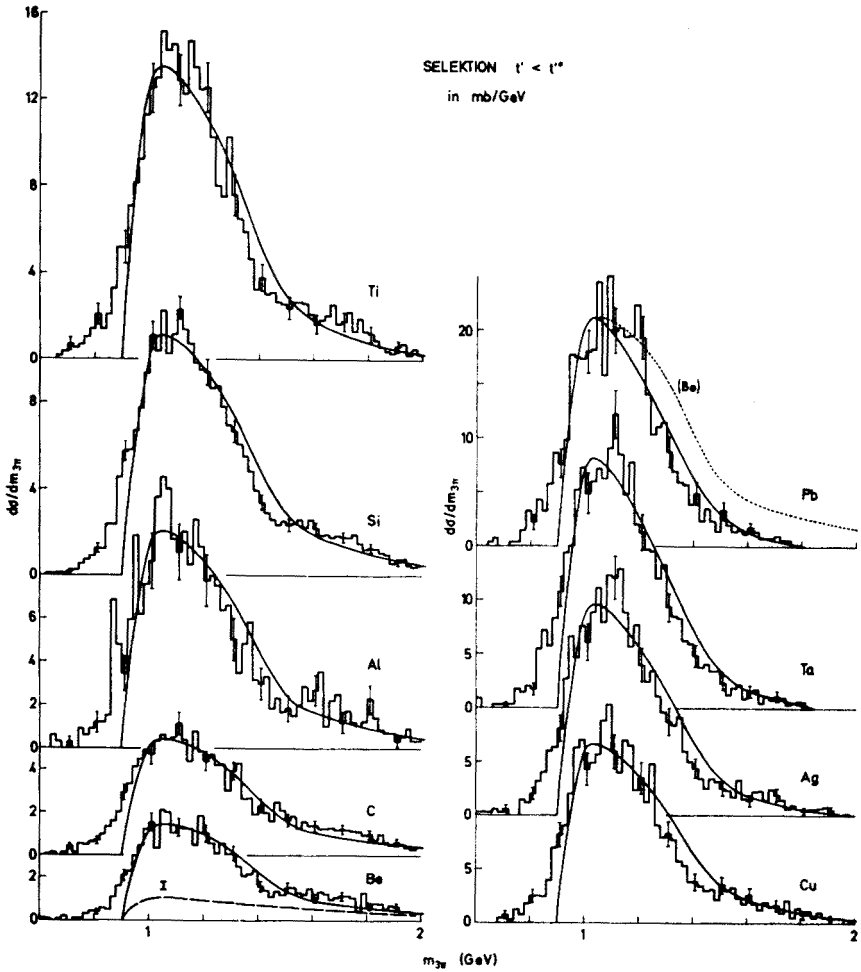

Fig. 10. 3π mass distribution for the nine target nuclei. The curve is a phenomenological model [11] modified for the effect of the nuclear form factor

We now turn to other properties of the coherently produced 3π system. How far is the mass distribution independent of A? To compare different target nuclei we have to remove the effect of the nuclear form factor that increasingly depresses higher masses with increasing A. This comparison is shown in Fig. 10. A phenomenological model [11] for diffractive $\pi+\varrho$ production, modified for the nuclear form factor, is compared [12] to the data (see Fig. 10). The difference between the model and the data shows no A dependence *i. e.* the suppression of large 3π masses in heavy nuclei (see the Pb–Be comparison in Fig. 10) is due only to the nuclear form factor.

How do the 3π masses, produced coherently on nuclei, compare to those produced on free protons? Figure 11 shows a comparison of the coherent production at 15.1 GeV/c (all elements) with 3π production on free protons (compilation of hydrogen bubble

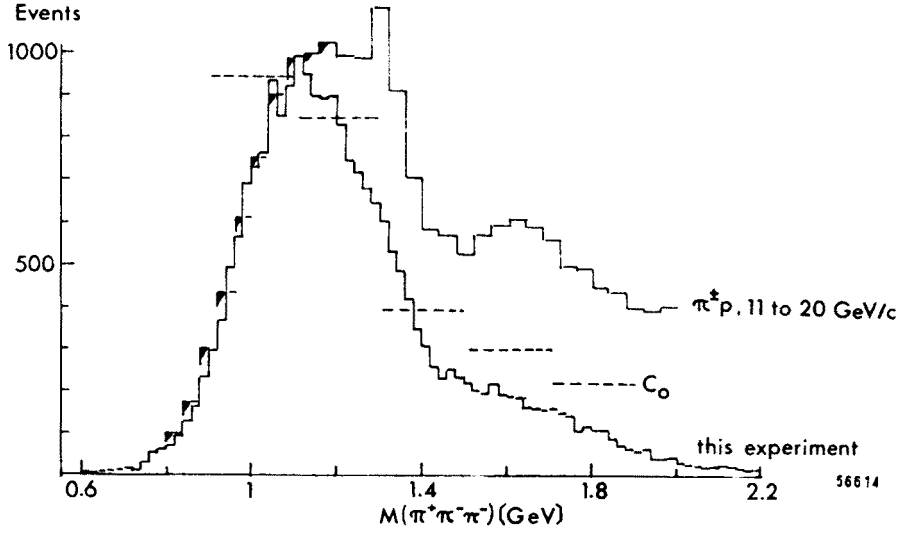

Fig. 11. 3π mass distribution (not corrected for acceptance) for all target nuclei at 15.1 GeV/c, with 20 MeV bins. Compilation of $\pi^{\pm}p \to (3\pi)^{\pm}p$ with 40 MeV bins [13]. C_0 is the forward production cross-sections on free nucleons (see text), corrected for acceptance

chamber events, p = 11 to 20 GeV/c [13]). Figure 11 shows agreement of the two mass distributions on the low mass side and deviation starting at the peak of the coherent mass distribution. In the 1300 MeV region, this difference is due to the A_2, present in the data on free protons, absent in coherent production. At higher masses the nuclear form factor suppresses the coherent data. The suppression factor may be inferred from the 200 MeV bins in Fig. 11. The height of these bins is proportional to $C_0(M)$ (see Eq. (2)) which is obtained from fitting the coherent production model to all elements. $C_0(M)$ is the differential cross-section for diffractive production at zero scattering angle; all form factor effects are excluded from this quantity. At higher masses $C_0(M)$ lies always lower than the proton data, in particular, it shows no sign of an enhancement in the A_3 region (1640 MeV) as do the proton data. We must conclude that the A_3 is not present as a distinct peak in coherent production on heavy nuclei, in contrast to its production on protons and on deuterium [14]. As the values of $C_0(M)$ in Fig. 11 show, this absence of a peak is not explained by the nuclear form factor. We have also checked that the acceptance of the apparatus (see Fig. 3) has no rapid variation in this region of the particular f^0 decay distribution resulting from the decay of the A_3 with $J = 2$ and helicity $\lambda = 0$ decaying into πf^0 in a relative S-wave. We observe, however, copious πf^0 production in this mass region.

Let us consider next 2π mass distributions of the 3π system. Two combinations enter the $\pi^+\pi^-$ mass plot. If there is a dynamic effect in one $\pi^+\pi^-$ combination (*e. g.* the ϱ^0) it will influence also the other one. In Fig. 12 a clear ϱ peak is visible, whereas the shaded $\pi^-\pi^-$ mass distribution shows no structure. Selecting 3π masses above 1.5 GeV an f^0 peak emerges with an area comparable to that of the ϱ peak.

How diffractive is coherent production? The longitudinal phase space (LPS) analysis [15] has been shown in many experiments to be a good tool for separating different reaction mechanisms contributing to the same multibody final state. Since we know that coherent production on nuclei proceeds by a reaction mechanism where the quantum numbers of the vacuum are exchanged, we can reverse the argument and consider the LPS plot of

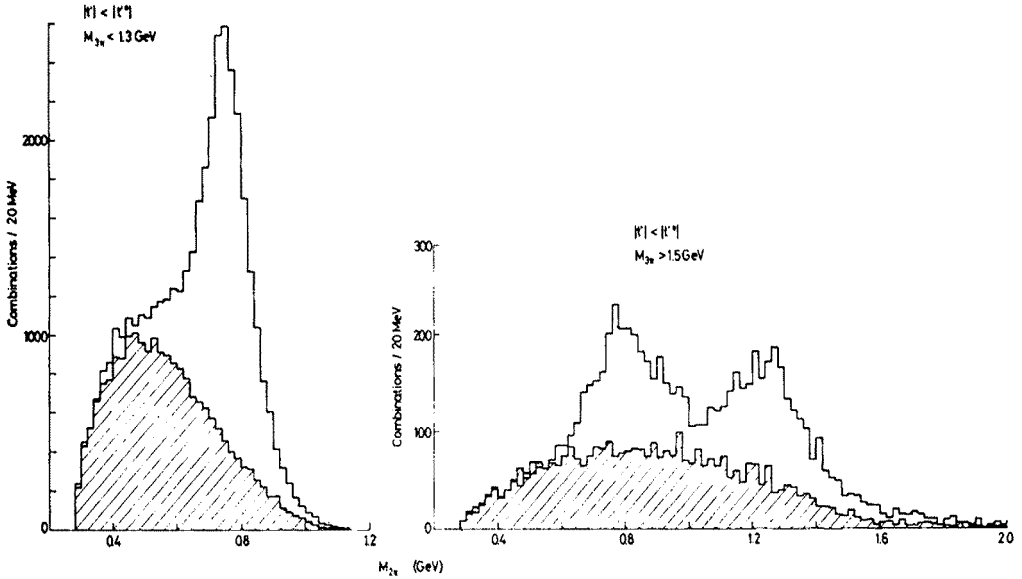

Fig. 12. 2π mass distribution for coherent events. The unshaded histograms are for the two $\pi^+\pi^-$ combinations, the hatched ones for the $\pi^-\pi^-$ mass. The distributions are compiled for all target elements

coherent production as an experimental test of the ideas behind the LPS analysis. Such a plot is shown in Fig. 13 [12]. The coherent events ($|t'| < |t'^*|$) are all contained within the triangle assigned to Pomeron or neutral meson exchange; also the incoherent events ($|t' > |t'^*|$) essentially show this pattern. The kinematics was computed with the mass of the nucleus for coherent events and with the mass of a nucleon for incoherent events. The incoherent events are heavily biased by the trigger system; they can therefore not be compared to events in a hydrogen bubble chamber. The trigger system selects events in the Pomeron exchange triangle of the LPS.

Diffractive processes are characterized by a cross-section that is almost independent of energy: $\sigma \propto p^{-n}$, $n \approx 0$. The exact value of the exponent n is not easily determined from production experiments on free protons; it is not sufficient to compare cross-sections at different energies, say $d^2\sigma/dtdM$ of $\pi^-p \to \pi^+\pi^-\pi^-p$ for a given interval of t and of $M = M(\pi^+\pi^-\pi^-)$. Non-diffractive processes may also contribute to this differential cross-section. The problem can be solved by projecting out the $J^P = 1^+$ state of $\pi^+\pi^-\pi^-$ by a partial wave analysis and by considering the 1^+ production representative for the diffractive process. In this case, $n = 0.42 \pm 0.11$ has been found [16].

We have seen in Fig. 13 that the diffractive production of 3π states is confined to

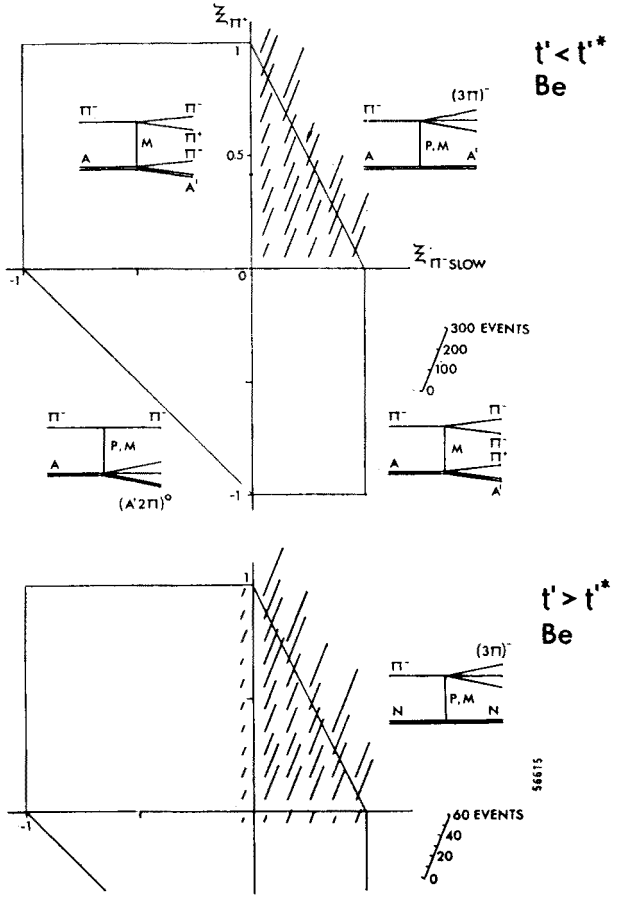

Fig. 13. Longitudinal phase space plot for 3π production on Be nuclei at 15.1 GeV/c, for mainly coherent (upper diagram) and mainly incoherent (lower diagram) events

a triangle in the LPS diagram. Hoping that the converse is also true, one can determine n for given regions of the LPS.

The ABBCH Collaboration [17] find n near zero or even negative (cross-section rising with energy) in a comparison of 8 and 16 GeV/c data. They argue that the cross--section of 3π production should at least fall off with energy as fast as that of elastic scattering. They consider, therefore, an exponent n, corrected for phase space effects, as the physically meaningful one. In the diffractive region: $n \approx 0.2$.

Considering again coherent production on nuclei to be purely diffractive, we can use the data at 9, 13, and 15 GeV/c do determine n. The differential cross-section for $\pi^- p(n) \to \pi^+\pi^-\pi^- p(n)$ at zero scattering angle is represented by $C_0(M)$. (Eq. (2), cross-sections on protons and neutrons assumed equal.) $C_0(M)$ is obtained with high precision from a fit over all nuclear targets; it depends, however, on the model of the nuclear form factor and its parameters. The preceding discussion has shown that the model is quantitatively correct, probably at least as well as partial wave and LPS analysis; moreover, the best fit values σ_2 turn out to be

essentially the same at 9 and 15 GeV/c (Table I), at least in the region where it is well measured. In Table III the energy dependence of $C_0(M)$ is shown. It is seen to rise with energy for all values of M, the $\pi^+\pi^-\pi$ mass.

TABLE III

Energy dependence of diffractive production cross-section. $C_0(M)$ is the forward point of $d^2\sigma/dt'dM$, integrated over the mass bin in question, units mb/(GeV/c)^2. Errors given are statistical only; there is a 4% change in $C_0(M)$ for a 1 mb change in σ_2 and a 1% change in $C_0(M)$ for α_2 going from 0 to −0.3. The exponent n is defined by $C_0(M) = \text{const}\ p_L^{-n}$. These results are preliminary

Mass bin (GeV)	σ_2 (mb)	$C_0(M)$ at momentum			Exponent n
		8.9 GeV/c	13 GeV/c	15.1 GeV/c	
0.9, 1.1	28	0.89±0.02	1.17±0.03	1.40±0.03	−0.87±0.1
1.1, 1.3	22	0.87±0.03	0.98±0.03	1.13±0.02	−0.5 ±0.1
1.3, 1.5	21	0.37±0.03	0.29±0.03	0.53±0.011	−0.68±0.2
1.5, 1.7	23	—	—	0.40±0.012	—
1.7, 1.9	13	—	—	0.29±0.013	—

This rise of the cross-section with energy is quite surprising. Should diffractive production behave differently, in that respect, from elastic scattering? Obviously one first has to check if this result is correct. Experimental errors I can think of are all quite small: efficiency corrections affect the data by 20% to 40% and the correction cannot be wrong by more than 10%; since the fit is acceptable for many target elements (with individual cross-sections determined), arithmetic errors are excluded. $C_0(M)$ is the $\theta = 0$ point of the differential cross-section. If one assumes $d\sigma/dt \propto e^{Bt}$, the minimum momentum transfer needed to produce a mass M depresses the $\theta = 0$ point for low energy; this effect is 6% between 9 and 15 GeV for $M = 1.3$ GeV and $B = 10$ (GeV/c)^2, much less than the observed rise. The analysis of diffractive production on free protons necessarily uses an integrated forward cross-section, whereas our analysis is restricted to very small t and essentially determines $d\sigma/dt'$ at $t' = 0$. Our result is therefore not in disagreement with the LPS analysis of Ref. [17], which also finds an increase of the diffractive production with energy in regions of the LPS which are most densely populated in coherent production (small t' and small $M(3\pi)$). Nearly constant or slightly falling integrated diffractive production cross-sections but increasing forward differential cross-sections would imply shrinking of the t' distribution.

3.3. Partial wave analysis of the 3π system

This experiment on coherent production has produced data that enable us to perform a very differential partial wave analysis of the 3π state. There are about 1000 events/20 MeV in the peak region; there are no complications at the nucleon vertex (no spin flip, no N^* production), and J^P is limited to the unnatural parity series only. The analysis is not yet finished. This section is therefore rather short and qualitative only.

The analysis is difficult and time-consuming, because there are too many events with too many variables. At fixed energy the final state is described by eight independent var-

iables. Fixing a mass bin $\Delta M(3\pi)$, integrating over t (no variation is expected in the small t interval of coherent production), and integrating over an uninteresting rotation around the beam axis, we are left with five independent variables. These variables are conveniently chosen as two coordinates, s_{12} and s_{13}, in the Dalitz plot and as the three Euler angles of the 3π system with respect to the Gottfried-Jackson frame (see Fig. 14).

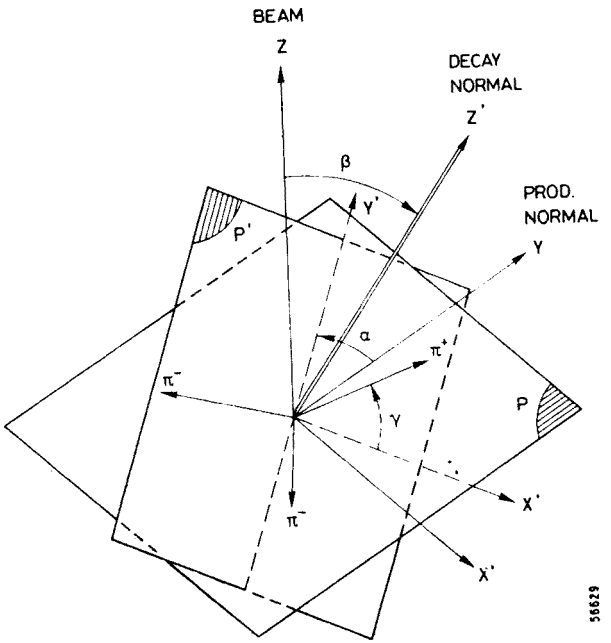

Fig. 14. Definition of the Euler angles α (in plane P), β and γ (in plane P')

The most powerful analysis method consists of fitting amplitudes which are functions of all five variables to the experimental data [18]. This method determines the density matrix elements for all states J^P and also their interference terms. The number of parameters to be fitted becomes very large and the analysis is very time-consuming, in particular, if it also has to take into account an acceptance as a function of five independent variables.

Partially integrated distributions are partially sensitive to the spin states. Distributions in α, β (angular distribution of the normal to the decay plane) are sensitive to the J^P of the 3π state and to interference between different J^P. Distributions in the Dalitz plot coordinates contain no interference between different J^P, but they are very sensitive to the presence of sub-states within a given J^P and to interference between such sub-states. The amplitudes in question have been given by Zemach [19]. They are somewhat model-dependent since the $\pi^+\pi^-$ final-state interactions are parametrized by Breit-Wigner amplitudes for ϱ, ε, and f^0; no final-state interaction for pions of like charge is assumed.

We have started with the analysis of the Dalitz plot distribution. In coherent production we are not so much interested in the density matrices of 3π production (we believe in the selection rules derived from spin and parity conservation). Rather, we are interested

in analysing the diffractive states of a given over-all J^P and in seeing how they are conditioned by final-state interactions (3π interaction, $\pi\varrho$, $\pi\varepsilon$, *etc.*).

The amplitudes for the states considered important are given in Table IV. The corresponding theoretical distributions are obtained numerically by Monte Carlo integration.

TABLE IV

Amplitudes for $\pi^+\pi^-\pi^-$ final states

3π state J^P	Two-body l	Amplitude
0^-	S	$BW_\varepsilon(1,2)+BW_\varepsilon(1,3)$
0^-	P	$BW_\varrho(1,2)\vec{p}_3\vec{t}_3-BW_\varrho(1,3)\vec{p}_2\vec{t}_2$
1^+	S	$BW_\varrho(1,2)\vec{t}_3-BW_\varrho(1,3)\vec{t}_2$
1^+	P	$BW_\varepsilon(1,2)\vec{p}_3+BW_\varepsilon(1,3)\vec{p}_3$
1^+	D	$BW_\varrho(1,2)t_{3k}T_{ki}(\vec{p}_3,\vec{p}_3)-BW_\varrho(1,3)t_{2k}T_{ki}(\vec{p}_2,\vec{p}_2)$
2^-	P	$BW_\varrho(1,2)T_{ij}(\vec{p}_3,\vec{t}_3)-BW_\varrho(1,3)T_{ij}(\vec{p}_2,\vec{t}_2)$
1^-	P	$[BW_\varrho(1,2)-BW_\varrho(1,3)]\cdot\vec{q}$
2^+	D	$BW_\varrho(1,2)T_{ij}(\vec{p}_3,\vec{q})-BW_\varrho(1,3)T_{ij}(\vec{p}_2,\vec{q})$

$\vec{p}_i$: momentum of π, in 3π CMS
$\vec{t}_i=\vec{p}_j'-\vec{p}_k'$, $i\neq j,k$, in $\pi_j\pi_k$ CMS
$\vec{q}=\vec{p}_1\times\vec{p}_2=\vec{p}_2\times\vec{p}_3=\vec{p}_3\times\vec{p}_1$
$T_{ij}(\vec{a},\vec{b})=\frac{1}{2}(a_ib_j+a_jb_i)-\frac{1}{3}\delta_{ij}\cdot\vec{a}\cdot\vec{b}$
BW_ϱ, BW_ε are relativistic Breit-Wigner amplitudes for ϱ, ε, respectively

The theory is very much influenced by the ambiguity between the two π^- present in the final state. Either π^- of the two can form a ϱ together with the π^+ and there is quantum mechanical interference. We are not allowed to choose a π^- "that is in the ϱ"; such a selection would be quite misleading. We cannot even expect to observe an undisturbed ϱ signal. Figure 15 shows the $\pi^+\pi^-$ mass distribution for various spin states and for two values of the 3π mass. In spite of the common input, namely a Breit-Wigner resonance amplitude ($m_s = 765$, $\Gamma_s = 135$ MeV), the theoretical $\pi^+\pi^-$ mass distribution turns out to depend on the angular momentum between π and ϱ and is generally different from what might be expected to be "ϱ+background". The amplitude even develops a high mass peak (Fig. 15b).

In the case of distinguishable particles the ϱ decay angular distribution is symmetric for pure states (and flat in the case of $\pi\varrho$ in relative S-wave). Figure 16 shows these distributions as a function of $\cos\chi_{+-}$, where χ_{+-} is the angle of the π^+ with respect to the "bachelor" π^- in the $\pi^+\pi^-$ CMS. The symmetrization required for our experiment makes all these distributions very asymmetric. If one would try to identify the "π^- in the ϱ" by a statistical ϱ selection, the background under this selection would still produce some skewness in the $\cos\chi_{+-}$ distribution that might then naively be explained by interference of two angular momentum states. The lesson to be remembered is: The only meaningful analysis consists in comparing a symmetrized theory to experimental distributions with two entries, one for each π^- present.

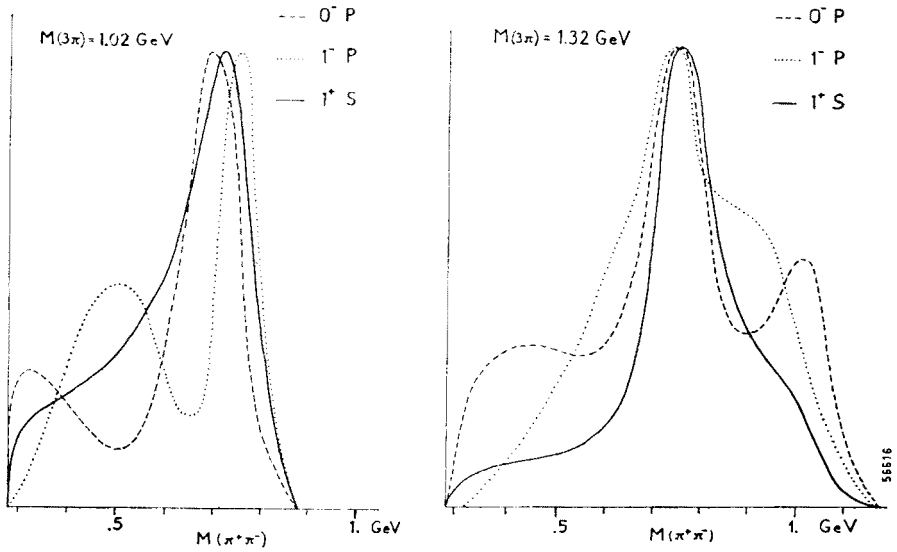

Fig. 15. Theoretical distribution of the $\pi^+\pi^-$ mass (two combinations) for $\varrho\pi$ in different angular momentum states

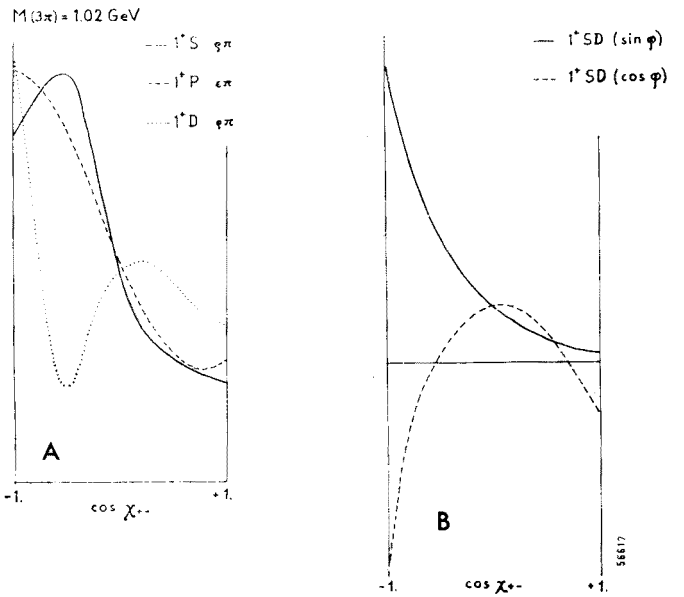

Fig. 16. Theoretical distribution of cos χ_{+-}, where χ_{+-} is the angle between the π^+ and the π_2^- in the $\pi^+\pi_1^-$ CMS (and indices 1, 2 reversed). A: pure 1^+ states, B: interference terms; φ is the relative production phase, the two distributions multiply sin φ, cos φ, respectively

As we have seen already, the over-all J^P of the $\pi^+\pi^-\pi^-$ system does not yet specify the Dalitz plot distribution. If we take the example of the predominant $J^P = 1^+$ state, it may be composed of $\pi-\varrho$ sub-states in S- or D-wave as well as $\pi-\varepsilon$ sub-states[2] in P-wave. Even small admixtures of P- and D-waves to the predominant S-wave may become important by interference. These interference terms are of a quite complicated structure. If we call the π^+ particle No 1 and the two π^- particles Nos 2 and 3 we have, for a single amplitude, say S-wave

$$A_S(s_{12}, s_{13}) = A_S(1, 2)+A_S(1, 3).$$

For two amplitudes, *e. g.* S and D, we have, leaving open a relative production phase, φ:

$$A_S+\exp\{i\varphi\}A_D = A_S(1, 2)+A_S(1, 3)+\exp\{i\varphi\}[A_D(1, 2)+A_D(1, 3)].$$

A_S and A_D are complex functions of the Dalitz plot coordinates s_{12} and s_{13}; the distribution arising from the interference term, W_{SD}, can be written as a sum of real functions W' and W'':

$$W_{SD}(s_{12}, s_{13}) = 2\cos\varphi\, W'_{SD}(s_{12}, s_{13})-2\sin\varphi W''_{SD}(s_{12}, s_{13}).$$

One-dimensional projections from such distributions are shown in Figs 16 and 17. On these figures the two terms are identified by (sin φ) and (cos φ), respectively. Since W' and W'' are different, the interference term not only changes magnitude as a function of φ but also its distribution on the Dalitz plot. Moreover, the interference does not vanish upon integration over the Dalitz plot.

Distributions of cos χ_{--} (χ_{--} is the angle between π^- and π^+ in the $\pi^-\pi^-$ CMS; these distributions must be symmetric) are shown in Fig. 17. Both the 1^- amplitude and the SD interference term multiplying sin φ have a prominent two-peak structure that is also found in the experimental data (see Fig. 18). This similarity may be the reason for some of the difficulties in the analysis of 3π final states[3]. In our data on coherent production the 1^- amplitude must be very small, since the coherent production of a vector meson vanishes in the forward direction (see Section 5). The two-peak structure of the data must therefore be explained by SD interference or $\pi\varrho(S)-\pi\varepsilon(P)$ interference which has a similar structure. So far, the analysis has not yet clearly distinguished between the two possibilities.

The likelihood function needed for the fit was constructed from the amplitudes given in Table IV. The goodness of the fit was then tested on the projection of the distributions onto the $m(\pi^+\pi^-)$, cos χ_{+-}, and cos χ_{--} axes; since there are only two independent variables, these projections are not independent. An example of such a fit is shown in Fig. 18. The structure in these projections gives evidence for the presence of interference terms in the $J^P = 1^+$ final state. This structure is particularly strong in the 1070 MeV region of the 3π mass.

The 0^- fraction ($\pi\varepsilon$ in S-wave) can be considered as a description of the non-resonating background. This amplitude is not unexpected since S-wave is clearly favoured near the

---

[2] We understand by ε a $\pi^+\pi^-$ S-wave with $I = 0$.

[3] The computer program given to us by a group at CERN did not contain the W'' term multiplying sin φ.

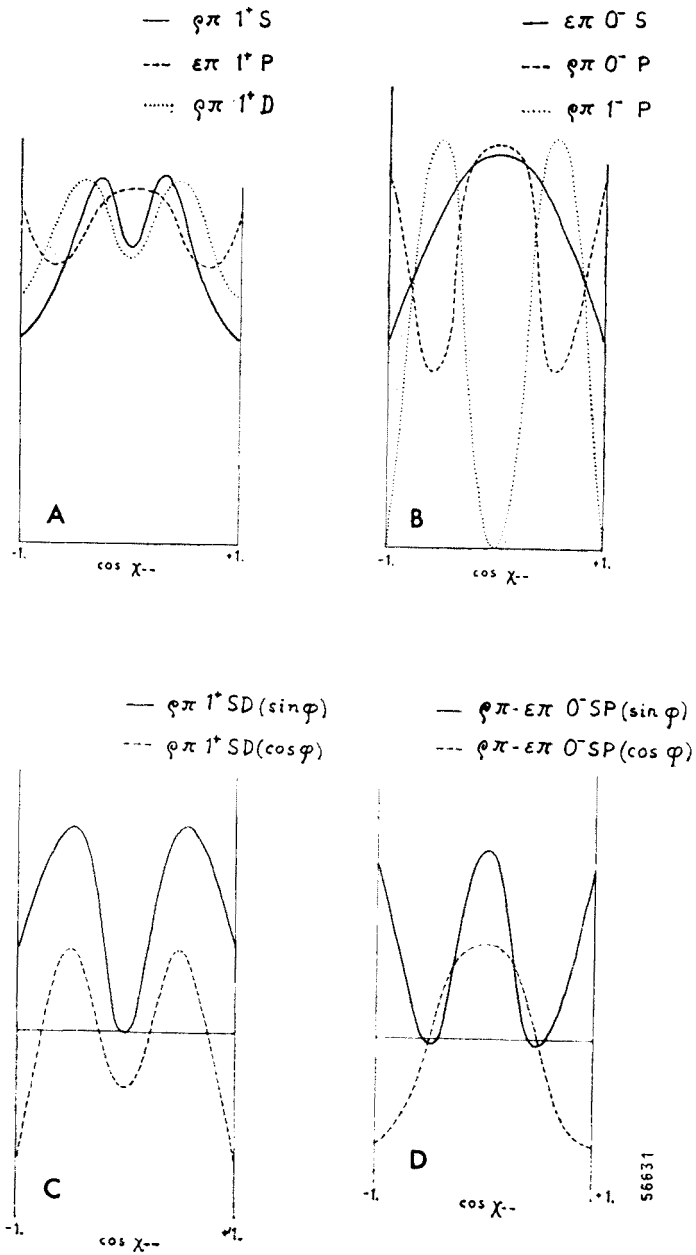

Fig. 17. Theoretical distribution of $\cos \chi_{--}$, where χ_{--} is the angle between π^- and π^+ in the $\pi^-\pi^-$ CMS; A: pure 1^+ states, B: 0^- and 1^- states, C: interference terms, D: $\varrho\pi-\varepsilon\pi$ interference terms. The meaning of (sin φ) and (cos φ) is explained in the caption of Fig. 16

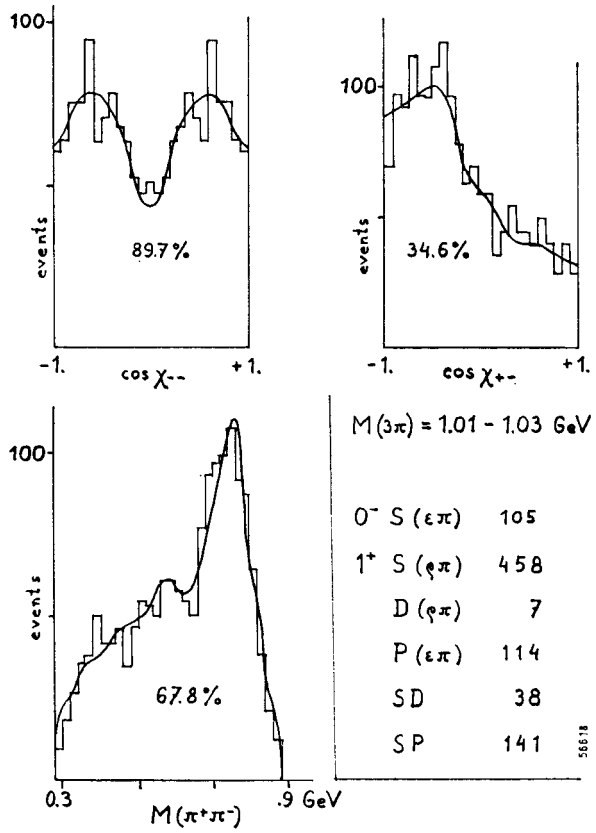

Fig. 18. Example of a fit of partial waves to experimental data. Preliminary, not corrected for acceptance. Percentage numbers are the χ^2 associated probabilities

threshold and since a strong $\pi^+\pi^-$ S-wave interaction with $I = 0$ does exist, be the ε a resonance or not. The $\pi\varrho$ D-wave, if confirmed, would be a rather narrow object ($\Gamma \lesssim 100$ MeV) in the 1070 MeV region. One might speculate that it is a genuine resonance, perhaps associated with the narrow object seen in bubble chamber data. We hope that further analysis, including also the variation of the acceptance over the Dalitz plot, will give us better evidence for D-wave and an unambiguous measurement of the $S-D$ relative phase. It would be quite interesting to see how a resonance — detectable only by its interference — could be hidden in this broad peak (see Fig. 11).

4. Diffractive $K\pi\pi$ production

4.1. Diffractive $K\pi\pi$ production, bubble chamber results

There is a complete similarity between diffractive 3π (A_1) and $K\pi\pi$ (Q) production. Figure 19 shows a compilation of $K^+p \to (K\pi\pi)^+p$ from 7.3 to 12.6 GeV/c [20]. A broad peak in the $K\pi\pi$ mass is observed which is quite similar to the 3π mass peak (see Fig. 11).

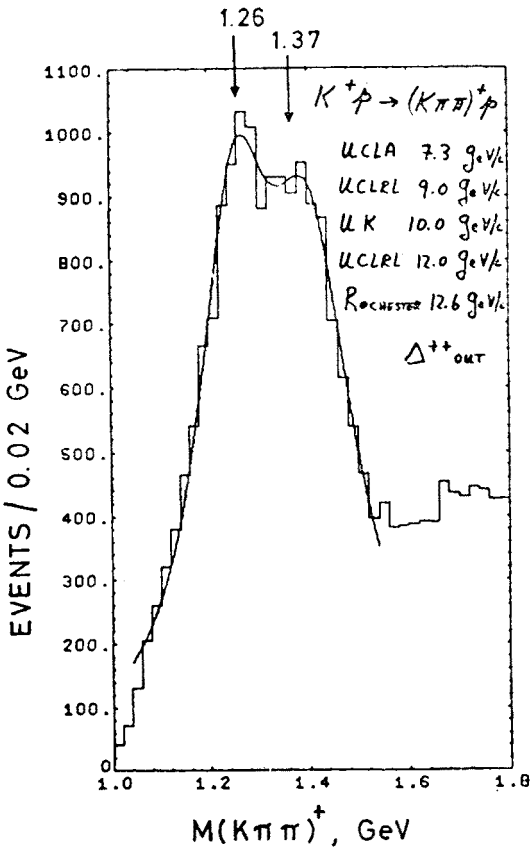

Fig. 19. Compilation of $(K\pi\pi)^+$ mass distributions by Firestone [20]

The peak cannot be fitted by a single Breit-Wigner. In the $K\pi\pi$ case it is not the $K^*(1420)$, the strange partner of the A_2, that produces a second peak. A fit with two incoherent resonances results in the following resonance parameters [19]

$$m_1 = 1250 \pm 4 \text{ MeV}, \Gamma_1 = 182 \pm 9 \text{ MeV},$$

$$m_2 = 1400 \pm 6 \text{ MeV}, \Gamma_2 = 220 \pm 14 \text{ MeV}.$$

The two resonances could correspond to the strange partners of A_1 and B. A_1 and B are distinguished by G-parity, which is not defined for strange mesons. Both can therefore be produced diffractively equally well. I do not understand, however, why these strange mesons should have Breit-Wigner mass distributions, while the A_1 has not.

Bubble chamber physicists have also been pioneers in the field of coherent $K\pi\pi$ production on nuclei. An example of results on complex nuclei [21] (propane-freon, Ne, $A \approx 20$) is given in Fig. 20. The characteristic "coherent" forward peak is very evident; its slope is compatible with the form factor of the nuclei in question if the angular resolution also is accounted for. The mass distribution of the events in the forward peak is shown in Fig. 21. The 12.7 GeV data are compared to 12.7 GeV data taken on free protons (Fig. 21b).

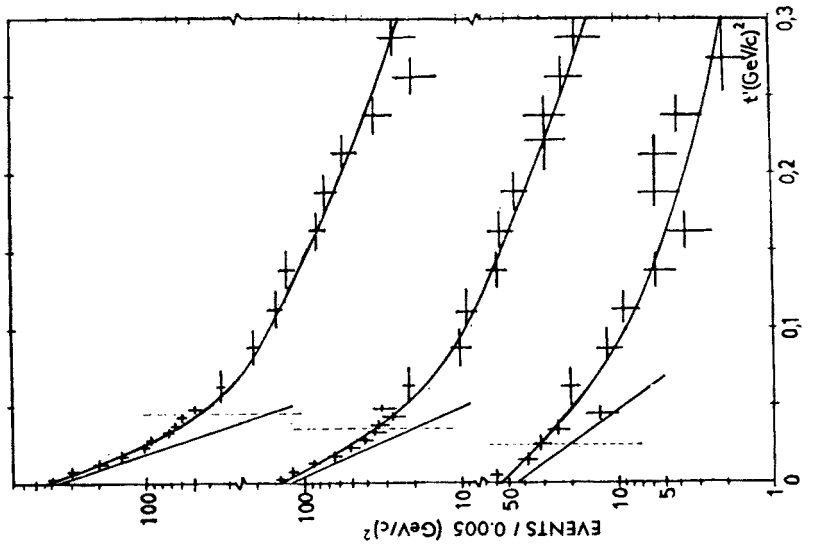

Fig. 20

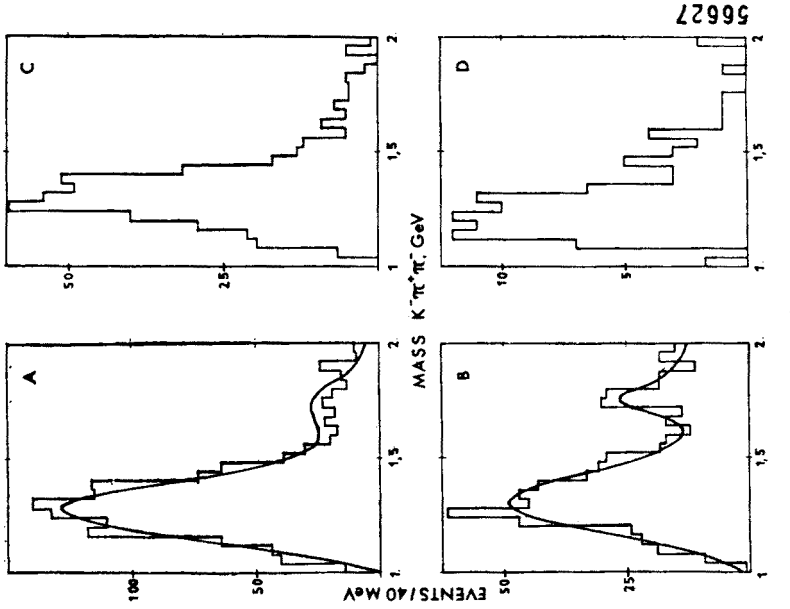

Fig. 21

Fig. 20. t' distribution of $K^-\pi^+\pi^-$ production at 12.7 GeV/c on Ne (top), at 10 GeV/c on freon-propane (centre), and at 5.5 GeV/c on Ne (bottom) [21]

Fig. 21. Mass distribution of coherently produced $K^-\pi^+\pi^-$ at 12.7 GeV/c (A), 10 GeV/c (C) and 5.5 GeV/c (D) and production on protons at 12.7 GeV/c (B)

The mass distribution on free protons gives a reasonable fit to the mass distribution observed in nuclei (Fig. 21a) when its modification due to the nuclear form factor is included.

Experiments on $K^{\pm}\pi^{+}\pi^{-}$ production at high energy suffer from an experimental difficulty: it is not always possible to distinguish K and π of the same charge. The statistical methods used to treat these ambiguous cases are quite questionable; moreover, they always assume that there is no systematic measurement error in the 4C-fit. Such systematic errors might have the effect that the wrong assignment gives a lower χ^2 of the fit than the correct assignment. It is therefore quite possible that the determination of the ratio $(Q \to K\varrho)/[Q \to K^*(890)\,\pi]$ has large systematic errors. The experiment in the heavy liquid bubble chamber [20] has determined this ratio also in a decay mode without experimental ambiguities: $Q^{-} \to \bar{K}^0\pi^{-}\pi^0$ (π^0 observed). The results are given in Table V. It may be significant that no background (*i. e.* neither K^* nor ϱ) is needed to fit the fully determined $\bar{K}^0\pi^{-}\pi^0$ channel.

TABLE V

Dalitz plot analysis of the $K\pi\pi$ system assuming $J^P, I = 1^+,0$ only (Ref. [21])

Channel	Beam (GeV/c)	Background (%)	$K^*\pi$ (%)	$K\varrho$ (%)	$K^*\varrho$ interference (%)
$K^0\pi^{-}\pi^0$	10 & 12.7	$1^{+\,10}_{-\,1}$	82 ±5	10 ±4	7 ±3
$K^{-}\pi^{+}\pi^{-}$	12.7	14± 5	62.5±4	13.5±4	10 ±4
	10	14± 7	65 ±5	11.5±4	9.5±3.5
	5	17±12	—	—	—

4.2. Coherent production of $K^{+}\pi^{+}\pi^{-}$: counter experiment

As a by-product of coherent $K^*(890)$ production (see Section 5) we have obtained a sizeable sample (15,000 coherent events) of $K^{+}\pi^{+}\pi^{-}$ coherent production on nuclei. This experiment should obviously be analysed along the lines presented in Sections 3.2 and 3.3. Since this is not yet done I shall present only a short and qualitative discussion.

The t' distribution of $K\pi\pi$ production shows exactly the same pattern as that of 3π production. t' is computed from the sum of the three meson momenta; it is not influenced by the mass assignment. Figure 22 shows this distribution; the two lines are the model fits to 3π production ($1 < m(3\pi) < 1.2$ GeV) shown for comparison. The small deviation near $t' = 0$ is explained by lack of angular resolution.

In this experiment there is essentially full ambiguity to the $K^{+}-\pi^{+}$ assignment. We found the most consistent results by choosing a K^* selection for this assignment, *i. e.* we chose as the K^{+} that positive particle which gives a $K^{+}\pi^{-}$ mass nearest to the $K^*(890)$ mass. This selection may seem very arbitrary; our high statistics distributions give, however, a very good idea of its effect as we will see later on. Figure 23 shows the distribution of the $K\pi\pi$ mass for "coherent" ($|t'| < |t'^*|$, see Section 3.2) and $|t'| > |t'^*|$ events. There is clearly no double-peak structure in the "coherent" events; the incoherent events produce a peak with a flat top, but also without structure. The similarity to the 3π mass distribution (Fig. 11) is very striking.

Fig. 22

Fig. 22. t' distribution of $K^+\pi^+\pi^-$ production on several nuclei at 13 GeV/c. Curves are the same as in Fig. 5 (3π production)

Fig. 23. $K^+\pi^+\pi^-$ mass distribution (raw data) for all nuclei and beam momenta. The distribution of incoherent events ($t' > t'^*$) is drawn in for comparison

At this point, let us look at the experimental justification for K^* selection. The distribution of the $K^+\pi^-$ mass is shown in Fig. 24. This is probably the K^* mass plot with the highest statistics and signal-to-noise ratio ever shown. The fitted curve shown is a Breit-Wigner resonance with a correction for the mass of the parent particle, the Q. Consider

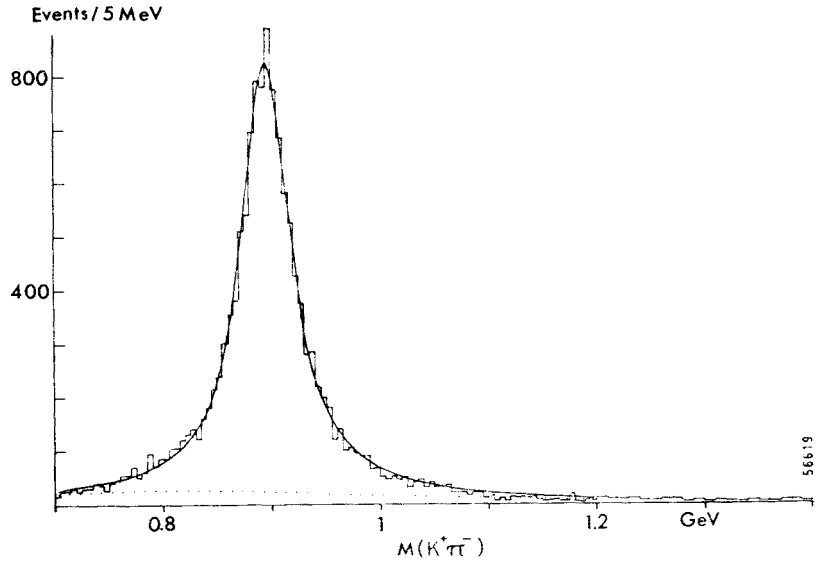

Fig. 24. Distribution of $K^+\pi^-$ mass for coherent events on all nuclei and at all beam momenta. The modified Breit-Wigner fit is explained in the text

a $K\pi$ mass bin on the high side of the K^*. For an event with very low Q mass this mass bin is forbidden by energy conservation, or at least suppressed by lack of phase space. The correction factor for mass bin $m_i(K\pi)$ was therefore taken as

$$\text{correction factor} = \sum_{j=1}^{N} \sqrt{\lambda\{m_j^2(K\pi\pi), m_i^2(K\pi), m^2(\pi)\}}\,,$$

λ being defined by Källen [22] and the sum going over all N events with masses m_j of the $K\pi\pi$ system. The fit of this corrected Breit-Wigner curve is excellent ($m = 899.2 \pm \pm 0.38$ MeV, $\Gamma = 57.4 \pm 1.2$ MeV)[4] and if we have forced genuine $\pi^+\pi^-$ events into the K^* band by our K^* selection, we have certainly done this very cleverly. Let us look now at the $\pi^+\pi^-$ mass distribution for the presence of any ϱ signal. Such a ϱ signal would obviously involve a crossing $K^*\varrho$ band in the Dalitz plot, since almost all $K\pi$ are in the K^* band. Figure 25 shows a very weak ϱ signal, if any at all, above a hand-drawn background. It is very instructive, in this case, to look at the K^* antiselection, *i. e.* the assignment of the π^+ mass to that positive particle of a $K^+\pi^-$ pair with the mass nearest to the $K^*(890)$. Figure 26 shows the $\pi^+\pi^-$ mass distribution in the case of K^* antiselection.

[4] The absolute value of the K^* mass may be wrong by a few MeV, due to uncertainty of the magnetic field map.

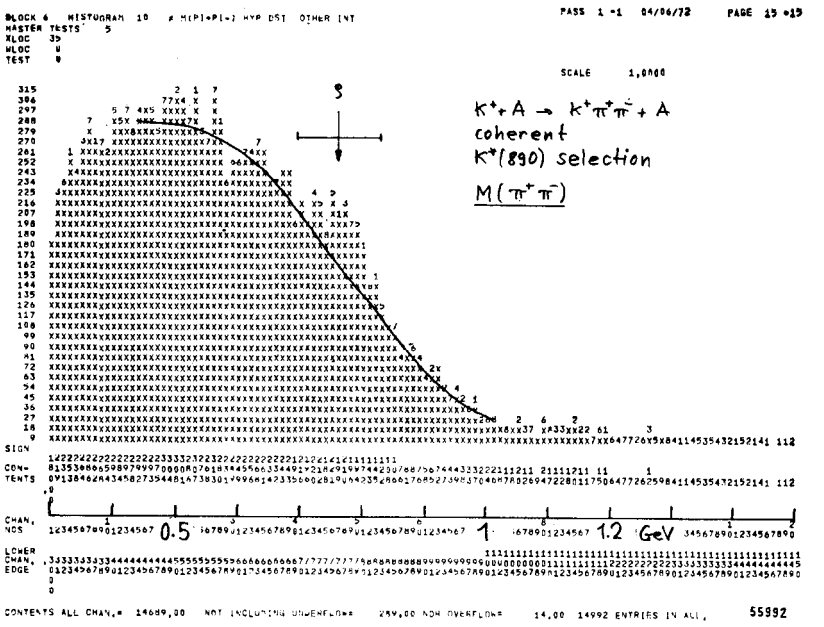

Fig. 25. Distribution of $\pi^+\pi^-$ mass for coherent events on all nuclei and all beam momenta (raw data)

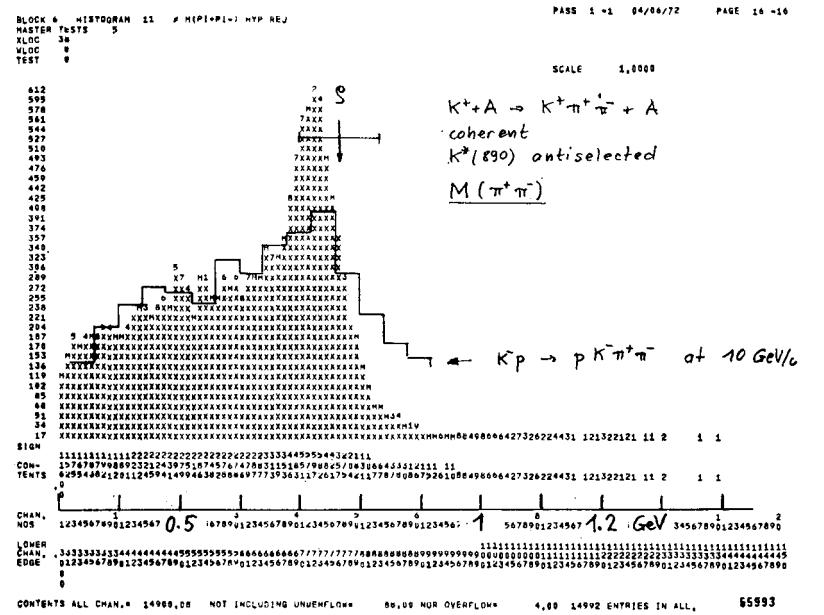

Fig. 26. Similar to Fig. 25, but π^+ mass assigned to the particle that was the K^+ previously. The peak is a reflection of the $K^*(890)$

A striking peak appears, which, at first sight (or in the case of small statistics) could be mistaken for a ϱ peak. Closer inspection reveals that it lies too low and is too narrow to be the ϱ peak. This peak is the effect of assigning the π^+ mass to the K^+ of a $K^*(890)$. The $\pi^+\pi^-$ mass distribution of a similar HBC experiment at 10 GeV/c [12] is drawn for

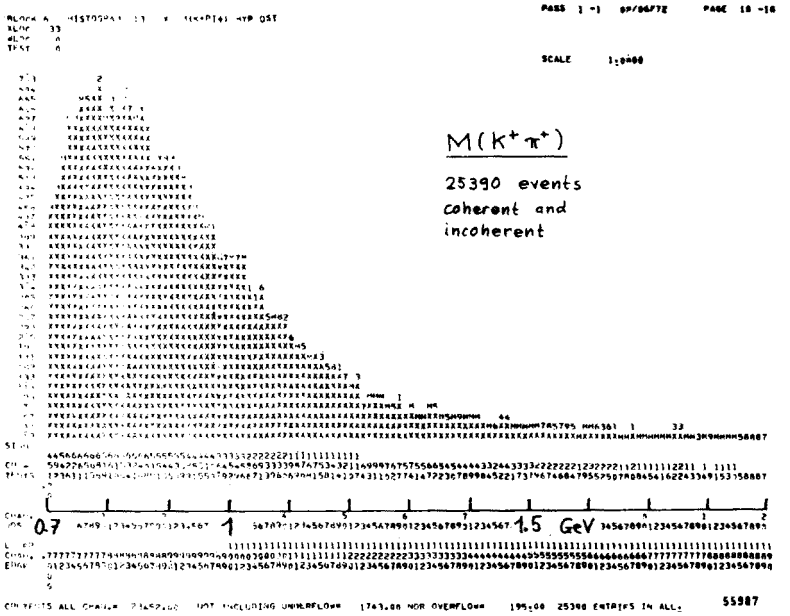

Fig. 27. Distribution of $K^+\pi^+$ for all events

comparison into Fig. 26 (rather than into Fig. 25 because it fits in so much better here; no further comment on this fact is offered). Finally, in the $K^+\pi^+$ mass distribution, shown in Fig. 27, there is no unexpected structure due to any exotic resonance.

5. *Coherent production of* $K^*(890)$ *on nuclei*

$K^*(890)$ production by incident K is not a diffractive process but it can be coherent, *i.e.* the production amplitudes on the nucleons of a nucleus interfere constructively. By this property, it has some relation to the subjects discussed at this School and I take the liberty of discussing it here. I shall discuss it in terms of γ and ω exchange, both having a spin and isospin independent part of the couplings. For spin-independent coupling (needed for coherence), conservation of spin and parity implies a zero of the amplitude in the forward direction. This can easily be shown in the helicity formalism, by the form of the Lorentz invariant coupling or by the following argument using angular momentum. Since the nucleus does not change its spin state in coherent production it can be considered as a spin 0 object. The initial state is then $|J_i, m_i\rangle = |l_i, 0\rangle$, both incident particles being spinless. In the final state we have

$$|l_i, 0\rangle = |J_f, 0\rangle = |l_f, m\rangle \oplus |l, -m\rangle.$$

Since there is no change in the intrinsic parities of the particles we have $l_i = l_f$. $|l_i, 0\rangle$ must be constructed from $|l_i, m\rangle$ and $|1, -m\rangle$. The Clebsch-Gordan coefficient for this addition vanishes for $m = 0$ ($2l_i+1$ is always odd). For $m = \pm 1$ the amplitude ($\sim Y_l^{\pm 1}(\Omega)$) has a sin θ factor and vanishes therefore in the forward direction. Coherent production, with its characteristic sharp forward peak, evidently suffers from this zero in the forward direction. It has been clearly observed, however [3,23].

Our experiment was planned to measure the Coulomb production of $K^*(890)$ (Primakoff effect) and its only unknown parameter, the partial decay rate $\Gamma(K^* \to K\gamma)$. The amplitude for this production is:

$$f_C(\vec{q}) = \sqrt{\frac{24\pi}{137}} \cdot \frac{m_{K^*}^{\frac{3}{2}}}{(m_{K^*}^2 - m_{K^+}^2)^{\frac{3}{4}}} \cdot Z \cdot [\hat{\varepsilon} \times \hat{k}] \cdot \frac{\vec{q}}{q^2} \sqrt{\Gamma(K^* \to K\gamma)}\, F_C(q^2). \tag{6}$$

$\hat{\varepsilon}, \hat{k}$ — polarization, momentum unit vectors of the K^*; $\vec{q}$ — momentum transfer; $F_C(t)$ — Coulomb form factor of the target nucleus (charge Z).

The Coulomb form factor can be expressed by

$$[\hat{\varepsilon} \times \hat{k}] \cdot \vec{q} \cdot F_C(q^2) = \int d^3\vec{r} e^{i\vec{q}\vec{r}} \cdot e^{-\frac{1}{2}\sigma(1-i\alpha)T(b)} \cdot e^{i\chi_C(b)} \times$$

$$\times [\hat{\varepsilon} \times \hat{k}] \cdot \nabla \cdot \int d^3\vec{r}' \frac{\varrho_e(\vec{r}')}{|\vec{r} - \vec{r}'|}. \tag{7}$$

The second integral, containing the charge density $\varrho_e(\vec{r}')$ normalized to 1 is the normalized Coulomb potential $\Phi(\vec{r})$. The Coulomb form factor (without absorption)

$$F_C(q^2) = \int \varrho_e(\vec{r}) e^{i\vec{q}\vec{r}} d^3\vec{r} \tag{8}$$

has to be transformed into an integral over $\vec{E}(\vec{r}) = \Delta\varphi(\vec{r})$ (using $\Delta E = \varrho$ and an integration by parts) in order to include the absorption term, $\exp\{-\frac{1}{2}\sigma(1-i\alpha)T(b)\}$. $T(b)$ is defined as in Eq. (3), but no distinction between incident and outgoing particle is made, as far as absorption is concerned. Equation (7) contains a six-fold integral because the whole charge distribution contributes to the $K \to K^*$ transition at the point $\vec{r}$. Due to the absorption and the Coulomb phase, the integration cannot any more be done in closed form. After some possible simplification [24] the integration is done numerically.

The Coulomb phase $\chi_C(b)$ is important in this experiment, since we will have to consider the interference of strong and electromagnetic production (and since $Z/137$ is of order 1). In general, for particles and target of the same sign:

$$\chi_C = -\frac{Z}{137v} \int_{-\infty}^{+\infty} \Phi(\vec{r}) ds, \tag{9}$$

where the integral is performed along the particle trajectory. This integral is divergent as it stands; the screening by the atomic electrons makes it finite and outside the charge distribution we find ($v \approx 1$)

$$\chi_C = -\frac{2Z}{137} \log(kb).$$

It is not difficult to compute $\chi_C(b)$ for the general case [25].

Let us look now at the strong amplitude. If the spin of the target does not enter into play, the Lorentz invariant amplitude must be of the form

$$f_{\text{str}}(\vec{q}) = [\hat{\varepsilon} \times \hat{k}] \cdot \vec{q} \cdot g(s, q^2). \tag{10}$$

This differs from a diffractive amplitude by the extra factor $[\hat{\varepsilon} \times \hat{k}] \cdot \vec{q}$. A comparison of the diffractive coherent production amplitude to coherent production derived from Eq. (10) can proceed as follows.

In the case of diffractive (A_1) production the form factor may be written

$$F_{\text{diff}}(q^2) = \int d^3\vec{r} e^{i\vec{q}\vec{r}} \int d^3\vec{r}' \delta^3(\vec{r} - \vec{r}') \varrho(\vec{r}'), \tag{11}$$

where the δ function is a consequence of a further simplification, namely, neglect of the q^2 dependence of $g(s, q^2)$ which is justified, *a posteriori*, by the much stronger q^2 dependence of the nuclear form factor. The production gets contributions only from the mass element $\varrho d^3\vec{r}$. This is very different from Coulomb production (Eq. (7)) in which case the whole charge distribution contributes.

The extra factor, $[\hat{\varepsilon} \times \hat{k}] \cdot \vec{q}$, of Eq. (10) gives rise to a gradient in the form factor of K^* production:

$$F_{K^*}(\vec{q}) = i \int d^3\vec{r} e^{i\vec{q}\vec{r}} \int d^3\vec{r}' [\hat{\varepsilon} \times \hat{k}] \cdot \nabla \delta(\vec{r} - \vec{r}') \varrho(\vec{r}') \tag{12}$$

to be compared to Eq. (11). Inserting absorption and the Coulomb phase, the amplitude for strong coherent K^* production becomes:

$$f_{K^*}(\vec{q}) = g(s) e^{i\varphi_0} A i \int d^3r e^{i\vec{q}\vec{r}} \cdot e^{-\frac{1}{2}\sigma(1 - i\alpha)T(b) + i\chi_C(b)} \times$$
$$\times [\hat{\varepsilon} \times \hat{k}] \cdot \nabla \varrho(\vec{r}), \tag{13}$$

where φ_0 has been inserted to account for the strong production phase, relative to Coulomb production. Integrating by parts one gets two integrals from the differentiation of the two exponentials:

$$I_0 = [\hat{\varepsilon} \times \hat{k}] \cdot \vec{q} \int d^3\vec{r} \cdot e^{i\vec{q}\vec{r}} e^{-\frac{1}{2}\sigma(1 - i\alpha)T(b) + i\chi_C} \varrho(\vec{r}) =$$
$$= [\hat{\varepsilon} \times \hat{k}] \cdot \vec{q} \cdot F_{\text{diff}}. \tag{14}$$

$$I_1 = -i[\hat{\varepsilon} \times \hat{k}] \int d^3\vec{r} e^{i\vec{q}\vec{r}} \varrho(\vec{r}) \cdot \nabla e^{-\frac{1}{2}\sigma(1 - i\alpha)T(b) + i\chi_C}. \tag{15}$$

At least one theoretician has written that I_1 is negligible with respect to I_0. We, of course, happily believed that and performed a full analysis using only I_0. The error was pointed out to us by Fäldt [26] and we (in particular, Freudenreich) had to restart the whole analysis.

Using the uniform sphere model of the nuclear density (radius R) one can simplify the integrals I_0 and I_1 and exhibit the difference ($\alpha = \chi_C = 0$ is used here)

$$I_0 = 4\pi[\hat{\varepsilon} \times \hat{k}] \cdot \frac{\vec{q}}{q_{||}} \int b db \sin(q_{||} \sqrt{R^2 - b^2}) J_0(q_\perp b) e^{-\frac{1}{2}\sigma T(b)} \varrho(0), \tag{16}$$

$$I_1 = 4\pi[\hat{\varepsilon}\times\hat{k}]\frac{3A\sigma}{4\pi R^3}\cdot\frac{\vec{q}}{q_{||}}\int\frac{b^3db}{\sqrt{R^2-b^2}}\sin(q_{||}\sqrt{R^2-b^2})\frac{J_1(q_\perp b)}{q_\perp b}\times$$

$$\times e^{-\frac{1}{2}\sigma T(b)}\varrho(0). \tag{17}$$

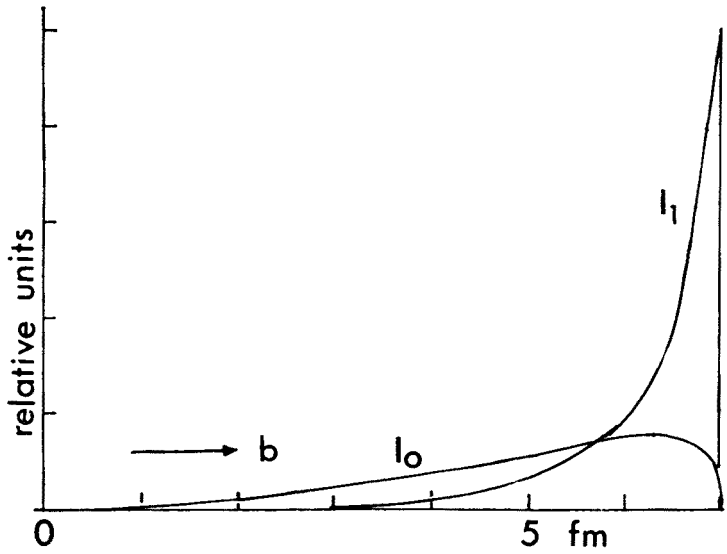

Fig. 28. Integrands of I_0 and I_1 (see text)

The integrands of I_0 and I_1 are plotted in Fig. 28 for comparison (small angle limit, $\sigma = 17$ mb, $R = 7$ fm). While both integrands vanish at $b = 0$ they differ widely at $b = R$. I_1 is in fact larger than I_0 (even more so at larger $q_\perp$) and the contribution to I_1 is concentrated at the nuclear surface.

For the final analysis of our data we have used the integral Eq. (13), using the Woods-Saxon density distribution. Since we have done the analysis twice, I shall also briefly comment on the results of the "wrong" analysis.

Let us finally look at the experimental data. The apparatus used was the same as that described earlier with the exception of a third Čerenkov counter added in the beam in order to identify K^+ safely (can the theoretical physicist reader find out why?). A difficulty of the experiment consisted in selecting the wanted $K^0\pi^+ \to \pi^+\pi^-\pi^+$ events from the much more abundant $K^+\pi^+\pi^-$ production. The extrapolation of the observed $\pi^+\pi^-$ trajectories to the K_S^0 decay vertex worked so well, however, that this selection produced neither contamination nor losses in the $K^*(890)$ sample. Figure 29 shows the t' distribution obtained on a Pb target, with the distribution for $\pi^- + \mathrm{Pb} \to 3\pi + \mathrm{Pb}$ drawn in for comparison. The forward zero in the K^* production amplitude cannot be actually observed due to limited angular resolution. Its effect is, however, visible as a flattening in the forward peak and as a much smaller relative height of the peak. The $K^*(890)$ signal (Fig. 30) is very clear and the background surprisingly low.

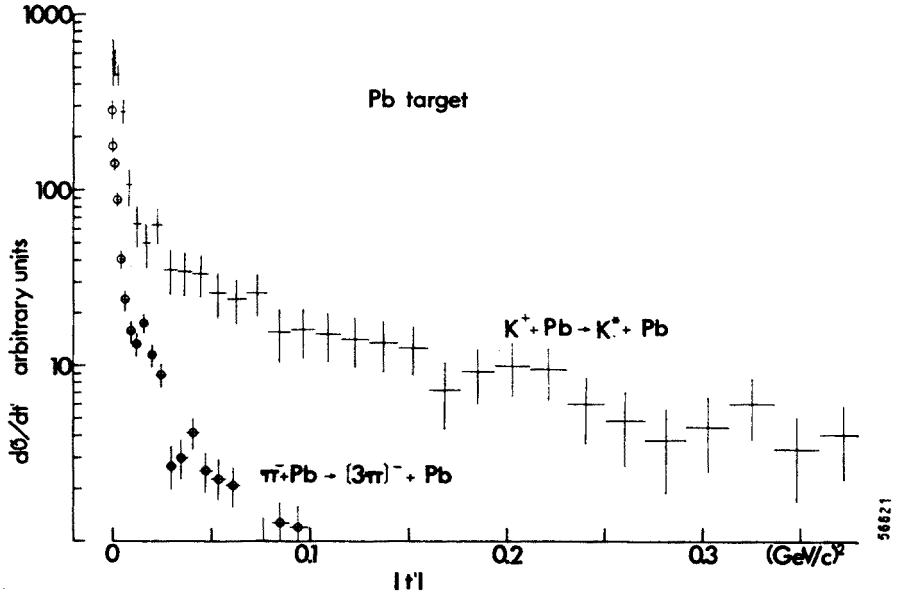

Fig. 29. Angular distribution $d\sigma/dt'$ for $K^*(890)$ production on Pb target. 3π production at 15.1 GeV/c is shown for comparison

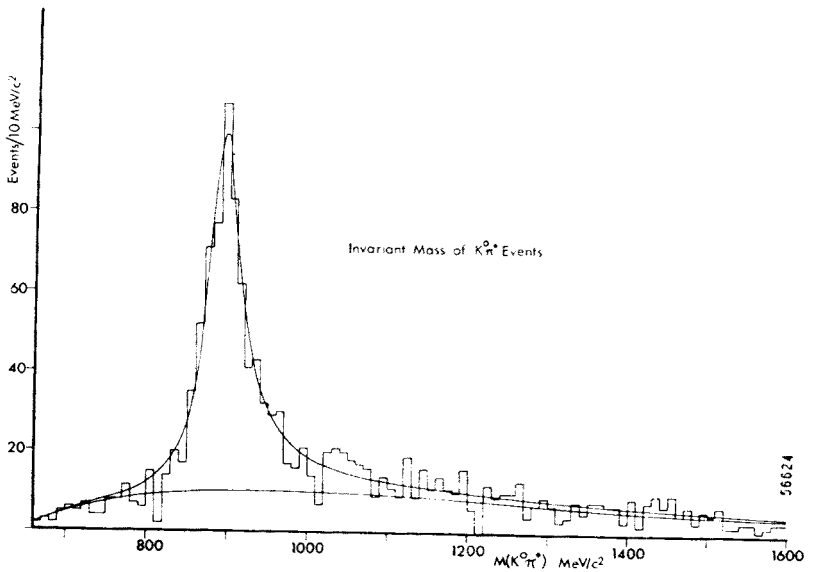

Fig. 30. Mass distribution of $K^0\pi^+$, all target elements and beam momenta

In principle, Coulomb production with the extra $1/q^2$ factor in the amplitude is separable from the strong K^* production by an analysis of the t distribution. Coulomb production is observable only on high Z elements (the cross-section is proportional to Z^2) and on these heavy elements the nuclear form factor has such a steep forward peak that the $1/q^2$ factor has a comparatively small influence. In order to observe the "Coulomb peak" one needs high resolution ($\Delta q_\perp \approx +10$ MeV/c) and high statistics, more than is available in our data. We have therefore used integrated coherent cross-sections σ_{coh} (see Eq. (5)) to distinguish between the two possible production mechanisms. In this case we rely on the A dependence and energy dependence of these cross-sections which follow from the model used for strong coherent production and which are therefore model-dependent.

The model cross-section is:

$$\frac{d\sigma}{dt'} = |f_{K^*}(\vec{q}) + f_C(\vec{q})|^2 + \frac{d\sigma}{dt'}\,(\text{incoh}). \tag{18}$$

The amplitude f_{K^*} is defined in Eq. (13), $g(s)$ is parametrized by $C^{\frac{1}{2}}(p/p_0)^{-n/2}$ (fit parameters C and φ_0) where $n = 1$ was taken as expected from ω exchange, $\sigma = 17$ mb and $\alpha = -0.26$ [28], and the Woods-Saxon parameters are as in Eq. (4). The Coulomb amplitude is defined in Eqs (6) and (7); its only fit parameter was $\Gamma(K^* \to K\gamma)$.

The 10 data points used in the fit are given in Table VI and the resulting fit parameters in Table VII.

Let us first discuss the A dependence of the strong production cross-section σ_{coh} (strong)

$$\sigma_{\text{coh}}(\text{strong}) = \int_0^{t'^*} |f_{K^*}(t')|^2 dt'.$$

This A dependence, for the 13 GeV/c data, is shown in Fig. 31. In the incomplete theory (I_0 only, Eq. (14)), the strong part of the cross-section decreases with A for $A \gtrsim 80$ (curve 0). Since the experimental cross-sections are rising in this region, the over-all fit

TABLE VI

Integrated coherent $K^*(890)$ production cross-sections

Target	Beam (GeV/c)	t'^* (GeV/c)^2	Events	σ_{coh}
Pb	15.8	0.0104	16	602 ± 150
C	15.8	0.0776	8	122 ± 43
Pb	12.9	0.0104	39	518 ± 82
Ag	12.9	0.0168	54	395 ± 53
Ti	12.9	0.0264	9	398 ± 132
Al	12.9	0.0448	10	245 ± 77
C	12.9	0.0776	12	143 ± 41
Pb	9.7	0.0104	58	601 ± 78
Ag	9.7	0.0168	30	575 ± 104
C	9.7	0.0776	12	125 ± 36

TABLE VII

Result of fitting Eq. (18) (see text) to the data points; integrated coherent cross-sections as given in Table VI

Number of data points (σ_{coh})	χ^2 degrees of freedom	$\Gamma(K^* \to K\gamma)$ (keV)	Upper limit of Γ, 95% confid. (keV)	φ_0
10	6.46 7	16^{+13}_{-16}	42	$-5°$
7 C excluded	3.26 4	28^{+34}_{-28}	77	$-6°$
5 C, Al, Ti excluded	1.0 2	37^{+35}_{-32}	87	$-8°$

needs a sizeable amount of Coulomb production leading to $\Gamma(K^* \to K\gamma) \approx 40$ keV. Having done this analysis we were very happy to have established a value for this parameter. But look now at the complete theory (I_0+I_1, Eqs (14) nad (15)). The theoretical A dependence is rather steeper than the experimental one with the consequence that $\Gamma(K^* \to K\gamma)$ is now lower and even compatible with being zero. The fit in Fig. 31 is systematically low because also data points at 10 and 16 GeV/c are included which force the model to give somewhat low values at 13 GeV/c.

The A dependence of the strong interaction coherent cross-section is not as well tested experimentally as that of 3π production (see Fig. 8). There is some weak evidence that the cross-sections of this model increase too fast with A. Therefore, some doubts remain

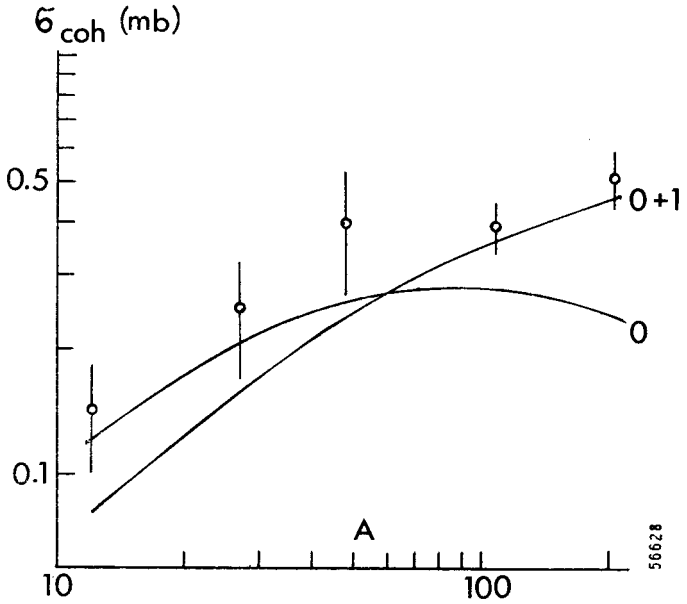

Fig. 31. Best fit optical model curves of strong interaction $K^*(890)$ production cross-section, and data on σ_{coh} at 13 GeV/c. The curve labelled 0+1 is the full theory, the curve 0 is a theory neglecting the second integral (see text). The best fit parameters of curve 0 are: $\Gamma(K^* \to K\gamma) = 39$ keV, $\varphi_0 = 79°$

about its validity, whereas the agreement with experiment in the case of 3π production is quite impressive. In what sense are the two models different? Coherent meson production on nuclei is a volume effect; only the absorption (which is not very strong) tends to decrease the production in the central part of the nucleus. It is quite natural that the optical model works so impressively well in this case. K^* production, however, is a surface effect proportional to $\nabla \varrho d^3\vec{r}$ rather than to $\varrho d^3\vec{dr}$. Only a few nucleons contribute in this case and the assumptions on which the optical model is based, may no longer be justified.

Having fitted the relative amounts of strong and of Coulomb production using the A and p dependence, we can compare now the predicted t' distribution with experiment. This is done in Figs 32 and 33. In Fig. 32 the contributions of Coulomb production (A), strong production (C), and the interference term B (negative beyond $t' = 0.004$ (GeV/c)^2), are shown separately. With the amount of Coulomb production determined by the fit, the sum curve D shows no peak at all at the lowest t', where Coulomb production would

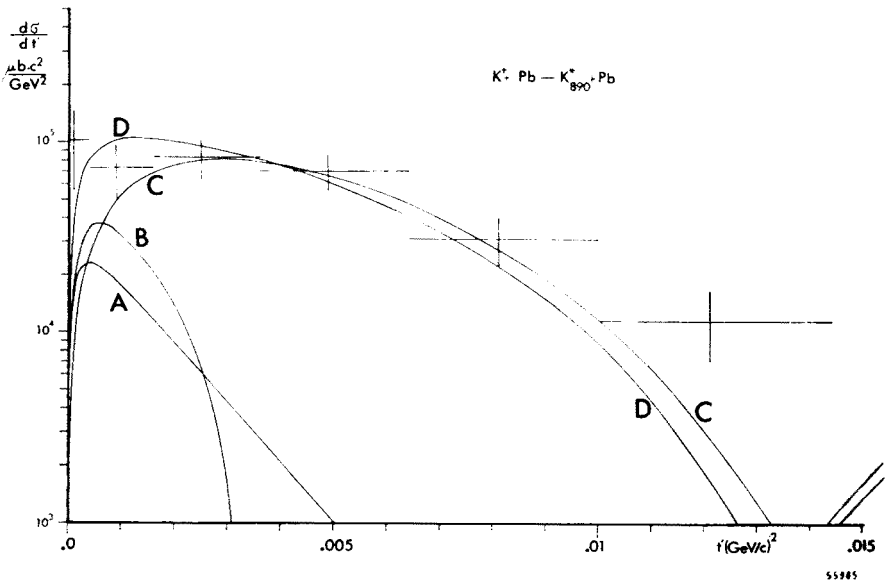

Fig. 32. Experimental and theoretical differential cross-sections for $K^*(890)$ production on a Pb target. A: Coulomb, C: strong production, B: interference term (negative beyond 0.0032 (GeV/c)^2). D: sum of A, B, C plus incoherent background. No t' dependence, but integrated cross-sections have been used in the fit resulting in curves A to D

be dominant. The diffraction pattern of the theoretical $d\sigma/dt'$ (see Fig. 33), not corrected for angular resolution, is not evident in the experimental data. We have seen (see Fig. 4) that this pattern is washed out if the angular resolution is $\Delta\theta \gtrsim 2$ mrad, which is the case here. In terms of t' dependence, the model is therefore in fair agreement with the data (remember: no fit on $d\sigma/dt'$ has been used) indicating that the model is not completely wrong, after all.

The results of the fits with parameters C, φ_0, and $\Gamma(K^* \to K\gamma)$ are shown in Table VII.

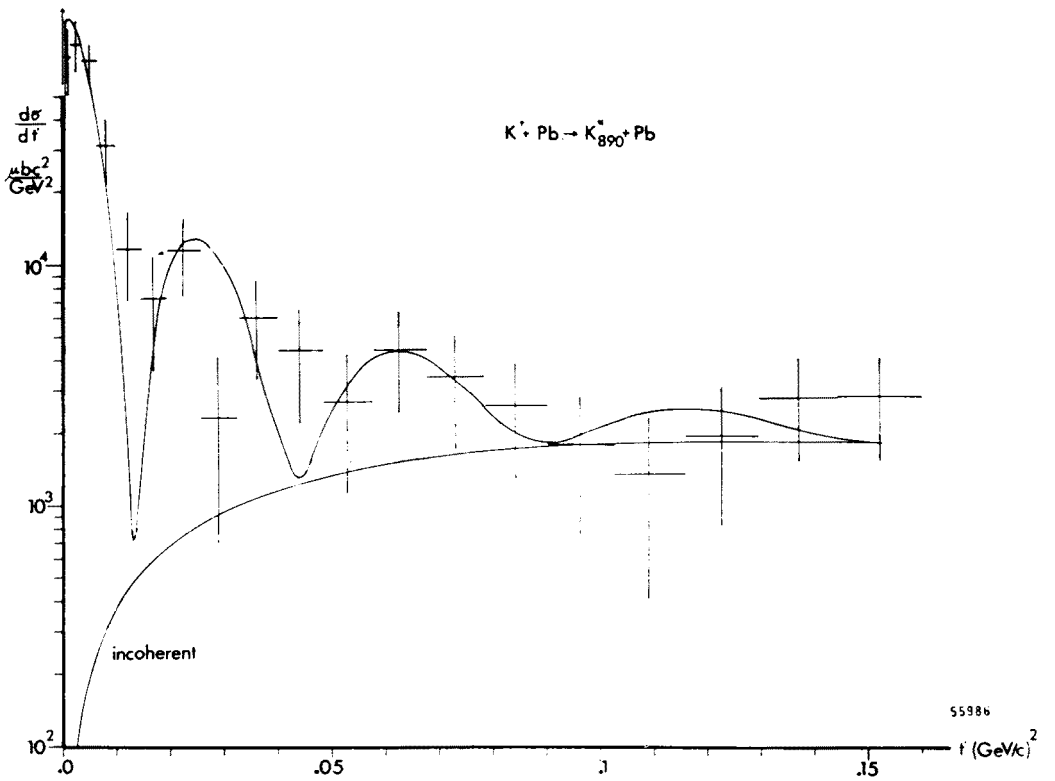

Fig. 33. Similar to Fig. 32. Only the sum curve is shown, not corrected for angular resolution

The systematic deviation between the experimental and the theoretical production cross-sections as a function of A leads to a large uncertainty in the determination of $\Gamma(K^* \to K\gamma)$ (for which the experiment was planned). Excluding low A target elements decreases the strong production cross-section. In view of these uncertainties, we prefer to give only an upper limit for the Coulomb production. With 95% confidence the radiative decay width is smaller than 80 keV. This upper limit is compatible with practically all recent predictions of this quantity [28].

The relative phase φ_0 between the strong and the electromagnetic production is not affected by the uncertainty on the A dependence (see Table VII). The χ^2 of the fit increases rapidly if the phase is changed from its best fit value in both directions. Our experiment seems to determine the phase of the strong production to be the same as that of the Coulomb production, *i.e.* a real production amplitude. A secondary minimum in the $\chi^2(C, \varphi_0, \Gamma)$, higher by 1.25 than the principal minimum, is found at $\varphi_0 = 162°$. This leaves the strong production amplitude still mainly real, but of an uncertain sign.

How does coherent K^* production on nuclei compare to K^* production on free protons? The comparison is more difficult here than in coherent A_1 production, since the fit parameter C (Eq. (18)) multiplies a function that vanishes in the forward direction.

For comparison we have to parametrize the data on free protons [29]

$$\left.\frac{d\sigma}{dt}\right|_p = C_p|t'|e^{-8|t'|} \quad \text{(GeV units)}. \tag{19}$$

We find, correcting for $K^* \to K^+\pi^0$, unobserved in Ref. [29], $C_p \approx 9$ mb(GeV/c)$^{-4}$. The fit to our data yields $C = 6 \pm 1.1$ mb(GeV/c)$^{-4}$. In view of the uncertainty of the parametrization (Eq. (19)) and of possible unnatural parity exchange contributions to the proton data, the agreement can be considered as quite satisfactory.

This experiment has obviously not answered all questions on coherent $K^*(890)$ production. How could it be improved? There is not much room for improvement at a 30 GeV accelerator. At higher energy one can hope to find a clear Coulomb production signal on a decreased strong production background. A condition for this is a sufficient angular resolution which implies the use of a thin target, *e.g.* 1 mm of Pb. It will therefore still be difficult to get sufficient statistics. We find 73 μb of Coulomb production cross-section at 16 GeV and expect therefore about 150 μb at 45 GeV. The observable cross-section ($K^{*+} \to K^0_S\pi^+$) is only 2/9 of that, *i.e.* 33 μb. About 10^{10} incident K mesons are needed to produce 1000 K^* by Coulomb production. This large flux may become feasible only with a 200 GeV accelerator. Since the kaons are a minority in the beam, either the spectrometer must be able to work in a very high flux, or the beam must be separated. We will probably have to wait some time for such an experiment.

I would like to express my gratitude to my colleagues of the CERN-ETH-Imperial College Collaboration, in particular to K. Freudenreich, L. Fluri, P. Mühlemann, J. Pernegr and W. Wetzel, who gave me the last results of their data analysis. I would also like to thank the organizers of the School for the friendly and stimulating atmosphere they created at the meeting in Zakopane.

REFERENCES

[1] C. Bemporad, W. Beusch, A. C. Melissinos, E. Polgár, D. Websdale, J. D. Wilson; J. P. Dufey, K. Freudenreich, R. Frosch, F. X. Gentit, P. Mühlemann; P. Astbury, J. Codling, J. G. Lee, M. Letheren; G. Bellini, M. Di Corato, G. Vegni, *Nuclear Phys.*, **B33**, 397 (1971).

[2] C. Bemporad, W. Beusch, A. C. Melissinos, E. Polgár, D. Websdale; J. P. Dufey, K. Freudenreich, R. Frosch, F. X. Genit, D. Mühlemann; J. Codling, J. G. Lee, M. Letheren, B. Bellini, M. Di Corato, G. Vegni, *Nuclear Phys.*, **B42**, 627 (1972).

[3] K. Freudenreich, R. Frosch, F. X. Gentit, P. Mühlemann; C. Bemporad, W. Beusch, J. P. Dufey, E. Polgár, D. Websdale, J. Wilson, O. Zaimidoroga; P. Astbury, J. Codling, J. G. Lee, M. Letheren, *Nuclear Phys.* **B**, in press.

[4] K. S. Kölbig, B. Margolis, *Nuclear Phys.*, **B6**, 85 (1968).

[5] For a review of coherent scattering on deuterium, see H. H. Bingham, *Acta Phys. Polon.*, **B3**, 31 (1972). For He recoil, see T. Ekelöf, B. Höistad, A. Åsberg; C. Busi, S. Dahlgren, A. J. Herz, S. Kullander, G. Lee, D. Websdale; G. Landaud, J. Younet, *Nuclear Phys.*, **B35**, 493 (1971).

[6] H. Palevsky, J. L. Friedes, R. J. Sutter, G. W. Bennett, G. J. Igo, D. W. Simpson, G. C. Phillips, D. M. Corley, N. S. Wahl, R. L. Stearns, B. Gottschalk, *Phys. Rev. Letters*, **18**, 1200 (1967). See also H. Palevsky, *Acta Phys. Polon.*, **B2**, 79 (1971).

[7] G. Bellettini, G. Cocconi, A. Diddens, A. N. Lillethun, E. Matthiae, J. P. Scanlon, A. M. Wetherell, *Nuclear Phys.*, **79**, 609 (1966).
[8] F. Bradamante, G. Fidecaro, M. Fidecaro, M. Giorgi, P. Palazzi, A. Penzo, L. Piemontese, F. Sauli, P. Schiavon, A. Vascotto, *Phys. Letters*, **31B**, 87 (1970).
[9] P. Astbury, G. Finocchiaro, A. Michelini, D. Websdale, C H. West, W. Beusch, B. Gobbi, M. Pepin, E. Polgár, M. A. Pouchon, *Nuclear Instrum. Methods*, **46**, 61 (1967), P. Mühlemann, J. D. Wilson, CERN 70-71 (1970).
[10] C. A. Engelbrecht, *Phys. Rev.*, **B133**, 988 (1964).
[11] V. J. Stenger, Institut für Hochenergiephysik, Universität Heidelberg, *Preprint* (1970).
[12] P. Mühlemann, *Thesis*, Diss. Nr. 4809, RTH, Zurich.
[13] D.R.O. Morrison, rapporteur's report, Proc. 15th Int. Conf. on High-Energy Physics, Kiev 1970, Preprint ITP-71-66E.
[14] K. Paler, R. C. Badewitz, H. R. Barton, D. H. Miller, T. R. Dalprey, J. Tebes, *Phys. Rev. Letters*, **26**, 1675 (1971).
[15] L. Van Hove, *Phys. Letters*, **28B**, 429 (1969).
[16] G. Ascoli *et al.*, Illinois-Genova-Hamburg-Milano-Saclay-Harvard-Toronto-Wisconsin Collaboration, *Phys. Rev. Letters*, **26**, 929 (1971).
[17] J. V. Beaupre *et al.*, Aachen-Berlin-Bonn-CERN-Heidelberg Collaboration, *Nuclear Phys.*, **B46**, 1 (1972).
[18] G. Ascoli, D. V. Brockway, H. B. Crawley, L. B. Eisenstein, R. W. Ranft, M. L. Ioffredo, U. E. Kruse, *Phys. Rev. Letters*, **25**, 962 (1970).
[19] Ch. Zemach, *Phys. Rev.*, **133B**, 1201 (1964).
[20] A. Firestone, in *Experimental Mesons Spectroscopy* (Eds. Ch. Baltay and A. H. Rosenfeld), Columbia University Press, New York and London 1970.
[21] B. Daugeras *et al.*, Orsay-BNL-Berkeley-Milano-Saclay Collaboration, submitted to the 4th Int. Conf. on High Energy and Nuclear Structure, Dubna, 7-11 September 1971.
[22] G. Källén, *Elementary Particle Physics*, Addison-Wesley, Reading, 1964.
[23] B. Daugeras *et al.*, Orsay-BNL-Berkeley-Milano-Saclay Collaboration, *Phys. Rev. Letters*, **27**, 1752 (1971).
[24] G. Morpurgo, *Nuovo Cimento*, **31**, 569 (1964).
[25] G. Fäldt, *Phys. Rev.*, **D2**, 846 (1970).
[26] G. Fäldt, *Nuclear Phys.*, **B43**, 591 (1972).
[27] G. Giacomelli, *Progr. Nuclear Phys.*, **12**, 77 (1970).
[28] G. Morpurgo in *International School of Subnuclear Physics "Ettore Majorana"*, Erice, Sicily (Ed. A. Zichichi), Academic Press, New York and London 1972.
[29] K. W. J. Barnham, D. C. Colley, M. Jobes, K. Pathak, L. Riddiford, P. M. Watkins, I. Griffiths, I. S. Hughes, I. McLaren, C. D. Procter, R. M. Turnbull, *Nuclear Phys.*, **B28**, 171 (1971).